Supporting Information

Is a catalyst always beneficial in plasma catalysis?

Insights from the many physical and chemical interactions

Table of contents

S1. Computational set-up of the DFT calculations

The microkinetic models, of which the results are presented in the main paper, require activation barriers and rate coefficients to calculate the rates of the corresponding reactions. For reactions occurring on the catalyst surface, the activation barriers are obtained from scaling relations (see section S2) and the corresponding rate coefficients are calculated from these barriers using transition state theory (see section S3). The scaling relations, which are used to calculate the activation barriers, are in turn derived from surface species energies calculated with density functional theory (DFT). Most of the surface species energies used to construct the scaling relations are taken from Schumann *et al*. [1] However, some additional species required in our DRM chemistry set, were not included in that paper, and are therefore calculated by ourselves with DFT, using settings that match those of Schumann *et al*. [1] as closely as possible, for consistency reasons. A list of these species with their corresponding energies and frequencies can be found in Table S1. Note that for gas-phase species (listed in

Table S2) the energies and frequencies are not calculated using DFT, but taken from the NIST chemistry webbook [2]. The computational details of our DFT calculations are discussed below.

Periodic plane-wave DFT calculations are carried out using the Vienna Ab-initio simulation Package (VASP version 6.2.1) [3–8]. We use the exchange-correlation functional BEEF-vdW (van der Waals corrected Bayesian error estimation functional) [9,10]. The core electrons are described by the projector augmented wave (PAW) method [11,12]. A plane-wave kinetic energy cutoff of 400 eV is used for the plane-wave basis set and the energy is converged within 10^{-7} eV. A Γ-centered 4×4×1 *k*-point mesh is used. Initial geometries of the adsorbed species are taken from the work of Schumann *et al.* [1] (i.e., a four-layer (3x3) fcc (111) slab with the top two layers allowed to move) as the DFT calculations are used to supplement their dataset. These geometries are relaxed with our computational setup to obtain total energies that can be used for the calculation of reaction and activation energies. Relaxing the geometries of the adsorbed species again (and not taking the optimized geometries from Schumann *et al.* [1]) is necessary because our computational setup is not completely identical to that work. Transition states are obtained using the dimer method, as implemented in the VASP Transition State Tools (VTST) [13–16] package, and are confirmed to be first order saddle points, as only one imaginary frequency is found in the normal mode analysis. The force on each atom is converged within 0.01 eV/Å.

S2. Surface kinetics simulations using the CatMAP code

The surface kinetics simulations (discussed in section 4.6 of the main paper) are performed with the mean-field microkinetic modelling software CatMAP, developed by Medford *et al* [17]. The software calculates reaction rates and fractional coverages at steady state for surfaces exposed to a fixed gas mixture. Specifically, the change in fractional surface coverage θ_s as a function of time, for species s on the catalyst surface is expressed as [17]:

$$\frac{\partial \theta_s}{\partial t} = \sum_{s,cat} \left[(c_{s,i}^R - c_{s,i}^L) r_{i,net} \right] = 0 \qquad \text{(S1)}$$

which equals zero at steady state. In eq. (S1), $c^R_{s,i}$ and $c^L_{s,i}$ are the stoichiometry coefficients of species s in reaction i for the right-hand (production) and left-hand side (destruction), respectively, and $r_{i,net}$ corresponds to the net rate of reaction i. The net rates are calculated from the fractional coverages, $\theta_{s,cat}$, for surface species, and from the partial pressure, $p_{s,cat}$, (which are kept constant) for gas species [17]:

$$r_{i,net} = k_i^f \prod_{s,cat} (\theta_s)^{c_{s,i}^L} \prod_{s,gas} (p_s)^{c_{s,i}^L} - k_i^r \prod_{s,cat} (\theta_s)^{c_{s,i}^R} \prod_{s,gas} (p_s)^{c_{s,i}^R} \qquad \text{(S2)}$$

in which k_i^f and k_i^r correspond to the forward and reverse rate constants, respectively. For more information on CatMAP, we refer to ref. [17].

While this model does not consider any changes in the gas composition due to e.g., gas or surface reactions, it allows to clearly illustrate trends in reactivity between different transition metals. These so-called activity plots display, for example, the production or destruction rates of a specific gas species as function of two descriptors. The descriptors are variables on which other parameters in the model, in this case the adsorbate and transition state energies, are dependent [17]. The use of these descriptors is made possible due to the existence of scaling relations, i.e., correlations between the adsorption energies of surface species and those of specific descriptor adsorbates [18,19]. In our simulations the O* and CH* binding energies are used as descriptors. The binding energies are defined as the formation energies of adsorbed O* and CH* relative to the empty slab and gaseous CO, H_2O and H_2. Note that, as long as the descriptors correlate well with the energies of the other surface species that bind to the catalyst via the O or C atom, the choice of the descriptors does not notably affect the results. The scaling relations used in our simulations are listed in Table S3, and are constructed using the adsorbate and transition state energies on transition metal (111) facets calculated by Schumann *et al* [1]. However, the energies of some surface species required in our simulations for CH_4/CO_2 were not included in that work and are thus calculated by ourselves, as described in section S1.

The simulations are executed at a temperature of 500 K and a total gas pressure of 1 bar, as these conditions are typical for DBD plasma. We employ the approximation that H* adsorbs on a separate reservoir site, as it is assumed to have negligible interactions with the other adsorbates because of its

small size [1,20]. As such H* can still co-adsorb even if the sites on which the larger species bind are fully covered. The Gibbs free energies of gas species are corrected using the Shomate equations. For gas species of which the Shomate parameters are not included in CatMAP by default, the parameters are taken from the NIST chemistry webbook [2]. The free energies of the surface species were corrected using the harmonic limit as implemented in the "Atomic Simulation Environment" (ASE) Python library [21]. The effect of radicals and stable plasma-produced species is investigated by setting small densities of these species in the gas mixture. If a radical is not included in the gas-phase, its adsorption and desorption reactions are removed from the chemistry set, to avoid net radical desorption from the surface due to the zero adsorption rate.

S3. Coupled plasma and surface kinetics simulations

Plasmas have a very rich gas-phase chemistry as a result of electron impact reactions, generating highly reactive species that subsequently react with each other or with stable gas molecules. As such, the plasma chemistry has a strong influence on the gas composition, and thus also on the surface chemistry of a catalyst in contact with this gas mixture. In turn, the destruction and formation of gas species on the catalyst affects the gas composition, and consequently the plasma. Hence, the plasma chemistry alters the surface chemistry and vice versa. Therefore, we developed a coupled plasma and surface kinetics model, which simultaneously calculates the number densities of gas species and fractional coverages of surface species as function of time.

S3.1 Balance equations of the surface and gas species

Our coupled model uses a continuously stirring tank reactor (CSTR) approach, meaning that perfect mixing is assumed in the reactor volume. As such, species densities in the plasma and surface coverages are considered uniform throughout the entire reactor. These densities and coverages change as function of time, as a result of chemical reactions, and due to reactants entering and products leaving the reactor.

The densities of the gas species are described by a balance equation:

$$\frac{\partial n_s}{\partial t} = R_{reaction,s} + \frac{n_{s,in} v_{in}}{V_{CSTR}} + \frac{n_{s,out} v_{out}}{V_{CSTR}} \quad \text{(S3)}$$

where n_s is the number density of species s, and t is the operating time. The first term on the right-hand side, $R_{reaction,s}$, denotes the change in number density due to reactions which is calculated according to eq. (S4), the second term corresponds to the feed gas entering the reactor and the third corresponds to the reaction mixture leaving the reactor. Here, $n_{s,in}$ is the species density in the feed, which is equal to 7.24×10^{18} cm^{-3} for CH_4 and CO_2, and zero for all other gas species, i.e., corresponding to a 1:1 CH_4/CO_2 gas mixture at 500 K and 1 bar. The volumetric flow rate entering the reactor, v_{in}, is chosen as 1.79 cm^3/s (corresponding to 107.4 mL/min for a typical DBD reactor), and the gas volume in the reactor, V_{CSTR}, is set equal to 8.85 cm^3. The gas mixture leaving the reactor, $n_{s,out}$, has the same composition as that in the reactor, $n_{s,out} = n_s$, and has a volumetric flow rate, v_{out}, which is calculated so that the total pressure in the reactor remains constant at 1 bar (10^5 Pa), as is shown below in eq. (S5).

The change in the number density of species s, as a result of reactions, is calculated by:

$$R_{reaction,s} = \sum_{i,gas} \left[(c_{s,i}^R - c_{s,i}^L) r_i\right] + n_{sites} f_{cat} \sum_{i,cat} \left[(c_{s,i}^R - c_{s,i}^L) r_i\right] + n_{sites}(1 - f_{cat}) \sum_{i,wall} \left[(c_{s,i}^R - c_{s,i}^L) r_i\right] \quad \text{(S4)}$$

Here, the first term on the right-hand side corresponds to the change due to reactions in the gas-phase, the second due to reactions on the catalyst surface, and the third due to interaction with a "non-catalytic"

wall. The latter can be, for example, the surface of the dielectric reactor wall or a dielectric packing. In eq. (S4), $c^R_{s,i}$ and $c^L_{s,i}$ correspond to the stoichiometry coefficients of species s in reaction i for production and destruction, respectively (which are at the right-hand side (R) and left-hand side (L) of the reaction equations, respectively). The reaction rates r_i are expressed in $cm^{-3}\ s^{-1}$ for gas reactions or s^{-1} for surface (catalyst or wall) reactions. The latter are therefore converted to the corresponding change in number density per unit of time (units of $cm^{-3}\ s^{-1}$) by multiplying with their volumetric site density. The number of catalytic sites per unit of gas volume is expressed as $n_{sites} \times f_{cat}$, where n_{sites} is the total volumetric site density of all (catalytic and wall) sites combined and f_{cat} is the fraction of these sites that are catalytic, i.e., transition metal sites. In our model, an estimated value of $1.5 \times 10^{18}\ cm^{-3}$ is used for n_{sites}, and the fraction of catalytic sites is set to 0.5 if a transition metal is present, or zero if this is not the case. As a reference, in ref. [22] de number of catalytic (metal) sites per mass of catalyst material was determined using CO pulse chemisorption for 5 wt.% transition metal catalysts on γ-Al_2O_3, and the measured values varied between 5-30 µmol/g (3-18 $\times 10^{18}$ sites/g). From our own observations we know that a DBD reactor with total (empty) volume of 17.7 cm^3 can hold about 12 g of γ-Al_2O_3-based catalyst pellets and that about half of the total volume of the packed reactor is occupied. As such, the gas volume, V_{CSTR}, in the reactor equals $0.5 \times 17.7\ cm^3 = 8.85\ cm^3$, as mentioned above. The parameters above correspond to volumetric site densities of 4-24 $\times 10^{18}\ cm^{-3}$. In our model, we use $n_{sites} = 1.5 \times 10^{18}\ cm^{-3}$, corresponding to a volumetric catalyst site density of $7.5 \times 10^{17}\ cm^{-3}$ for $f_{cat} = 0.5$. This is a factor 5.3 to 32 lower than aforementioned values, as we assume a smaller metal loading, i.e. 1 wt.% rather than 5 wt.%, and we use the lower end of the range to avoid overestimation of the effect of the catalyst. Indeed, we expect the effect of the catalyst to be slightly overestimated in our model, as we assume perfect mixing, while this is probably not true in reality, due to the short lifetime of the radicals, which might have reacted away before they are well mixed with the other gas species.

The volumetric flow rate of gas leaving the reactor, v_{out}, in eq. (S3) is calculated in such a way that the total pressure (and gas density) remains constant:

$$v_{out} = v_{in} + \frac{V_{CSTR} \sum_{s,gas} R_{reaction,s}}{\sum_{s,gas} n_s} = v_{in} + \frac{V_{CSTR} k_b T}{p_{tot}} \sum_{s,gas} R_{reaction,s} \qquad \text{(S5)}$$

As such, the volumetric flow rate that leaves the reactor, v_{out}, is equal to the sum of the volumetric flow rate entering the reactor, and the change in volume that results from the reactions under the chosen conditions of pressure and temperature. In eq. (S5), p_{tot} is the total pressure in the reactor, k_b is the Boltzmann constant and T is the temperature. Note that for simplicity the temperature of the gas, the catalyst surface and the wall are all assumed equal to 500 K, hence possible hotspots at the catalytic surface are neglected at this stage.

The fractional coverages and empty site fractions on the catalyst surface and wall are described by the following balance equations:

$$\frac{\partial \theta_{s,cat}}{\partial t} = \sum_{i,cat} \left[(c_{s,i}^{R} - c_{s,i}^{L}) r_i \right] \quad \text{(S6)}$$

$$\frac{\partial \theta_{s,wall}}{\partial t} = \sum_{i,wall} \left[(c_{s,i}^{R} - c_{s,i}^{L}) r_i \right] \quad \text{(S7)}$$

Like the simulations with CatMAP, we employ the approximation that H* binds on a separate site type, as explained in section S2. The catalytic sites are equally distributed between normal and H reservoir sites. Also on the non-catalytic wall, two types of sites are present, namely weakly binding physisorption and strongly binding chemisorption sites. Here, we choose a fraction of 2×10^{-3} for chemisorption and 0.998 for physisorption sites on the wall, based on refs. [23,24].

S3.2 Reaction rates

The reaction rates used in eq. (S4), (S6) and (S7) are calculated using the following equation:

$$r_i = k_i \prod_s (a_s)^{c_{s,i}^{L}} \quad \text{(S8)}$$

Here k_i is the reaction rate coefficient and a_s is the activity of species s, which is equal to the number density, n_s, for species in gas-phase reactions, and to the partial pressure, p_s, for gas species in surface reactions, or the fractional coverage, θ_s, for surface species. Number densities are converted to partial pressures and vice versa using the ideal gas law.

S3.3 Rate coefficients of gas-phase reactions

An overview of all gas and surface species in the model can be found in Table S4. Note that we do not include any vibrationally excited molecules, as their effect is negligible compared to that of radicals at the low temperatures that are typical for a DBD reactor (~ 500 K), as discussed in section 4.3 of the main paper. The rate coefficients, k_i, of the gas-phase reactions (with exception of electron impact reactions) are taken from literature and are listed in Table S5, together with the corresponding references. The rate coefficients of electron impact reactions are calculated as described in section S3.4.

S3.4 Rate coefficients of electron impact reactions

While electrons are not explicitly included as a gas-phase species, we obviously do include electron impact dissociation reactions as a way of generating radicals. The rate coefficients of these electron impact reactions are kept constant throughout the simulation. We note that this is a clear approximation for DBD plasmas, which typically consist of microdischarges and are hence non-uniform in both space and time. However, the goal of this study is to illustrate how the production of radicals and stable intermediates in the gas-phase can affect the surface chemistry and how the surface processes can alter the gas composition. A detailed treatment of the pulsed behavior of a DBD plasma combined with a catalyst is therefore outside the scope of this study, but will be investigated in future work.

The rate coefficients for electron impact processes are estimated as follows. First, we calculated the reduced electric field (E/n) at breakdown in pure CO_2 and CH_4 using the Paschen curves [25,26]:

$$\frac{E}{n_{tot}} = \frac{Bk_bT}{C + \ln(p_{tot}d)} \; with \; C = lnA - ln\left(ln\left(\frac{1}{\gamma} + 1\right)\right) \quad \text{(S9)}$$

Where A and B are experimentally determined parameters, taken from literature [25,26], and d is the size of the discharge gap, assumed here to be 4.5 mm. A value of 0.1 was assumed for the secondary electron emission coefficient γ. Typical values of γ in discharges are in the range of 0.1-0.01 [25,26]. Using γ = 0.01, however, results in a rise of only approximately 10% of the E/n calculated for these conditions. Using the Paschen curves, we find an E/n of 154 and 304 Td, for CH_4 and CO_2, respectively. We use the weighted average of these values, E/n = 229 Td, as a rough estimate of the electric field in the discharge for the 1:1 CH_4/CO_2 feed gas. Next, we calculate the rate coefficients of various electron impact reactions using BOLSIG+, a numerical solver for the Boltzmann equation for electrons [27]. We perform the calculation using a gas mixture containing 48.5% CO_2, 48% CH_4, 1.5% CO, 0.5% C_2H_6, 0.5% H_2O and 1.0% H_2. Small fractions of product species are included, as we also include their electron impact dissociation rate coefficients in the model. Note that the exact CH_4 and CO_2 conversions assumed for this gas mixture, and the corresponding fractions of product species, are not of great importance, as we found that the electron impact rate coefficients, calculated as described in this section, vary very little for different compositions. As such, the rate coefficients are considered constant throughout the simulations and do not change with rising conversion. A list of the electron impact processes included in the BOLSIG+ calculations can be found in Table S6. We assume an electron density of 10^{14} cm^{-3}, which is in the range of typical electron densities in the microdischarge filaments of a DBD [26]. We use this value as we will first calculate the electron impact rate coefficients in the microdischarges, which we will correct afterwards to account for microdischarges only taking up a small fraction of the gas volume, as described below. Apart from the rate coefficients of the electron impact processes, BOLSIG+ also provides the reduced electron mobility, $\mu_e \times n$, as function of E/n. The electron mobility, μ_e, can be related to the reduced electric field through:

$$\frac{E}{n_{tot}} = \frac{1}{n_{tot}}\sqrt{\frac{P}{n_e e \mu_e}} \quad \text{(S10)}$$

with P the power density, n_e the electron density and e the elementary charge. Reorganizing gives an expression for the power density:

$$P = E^2 n_e e \mu_e \quad \text{(S11)}$$

If we assume all power is deposited in the discharges, we can estimate the average combined volume of the microdischarges V_{plasma}, for a plasma power of 65 W. Since only a fraction of the gas molecules in the reactor will be exposed to this power density at a given point in time, we correct the electron impact

rate coefficients by multiplying with a geometrical factor V_{plasma}/V_{CSTR}. In Table S7, we list these corrected rate coefficients multiplied by the assumed electron density ($n_e = 10^{14}$ cm^{-3}).

We acknowledge that calculating the electric field by taking the weighted average of electric fields at breakdown for CH_4 and CO_2 gives only a very crude estimation of E/n. However, we find that if the rate coefficients are calculated according to the procedure described above, their values only vary by a factor 1 to 3 when comparing rate coefficients calculated with E/n = 154 Td (pure CH_4), E/n = 304 Td (pure CO_2) and E/n = 229 Td (weighted average). As such, the uncertainties on these rate coefficients are within the typical range of uncertainty factors for gas-phase reactions in literature [28].

S3.5 Rate coefficients of reactions on the catalyst surface

The catalyst surface reactions included in the model are listed in Table S8. The rate coefficients of these reactions are calculated using transition state theory:

$$k = \frac{k_b T}{h} \exp\left(-\frac{\Delta G^{\ddagger}}{RT}\right) = \frac{k_b T}{h} \exp\left(-\frac{\Delta \mathrm{H}^{\ddagger}}{RT}\right) \exp\left(\frac{\Delta \mathrm{S}^{\ddagger}}{R}\right) \quad \text{(S12)}$$

In which h is Planck's constant, R is the ideal gas constant and $\Delta G^{\ddagger}$, $\Delta H^{\ddagger}$ and $\Delta S^{\ddagger}$ are the differences in Gibbs free energy, enthalpy, and entropy, respectively, between the transition state and the initial state. The enthalpy differences are calculated from the species energies acquired from the scaling relations in Table S3. The thermodynamic corrections on the enthalpies and entropies are calculated using the Shomate equations for gas species and the harmonic approximation for surface species, as is also the case for the CatMAP code, discussed in section S2. Note that the rate coefficients calculated with eq. (S12) are expressed in s^{-1}. Specifically for these rate coefficients, the partial pressures used in the calculation of the reaction rates (eq. (S8)) need to be expressed relative to the standard state pressure of the gas (1 bar).

The rate coefficients for adsorption reactions are limited by the gas kinetics multiplied by a sticking coefficient that is function of the activation enthalpy:

$$k_{ads} = \frac{A_s}{\sqrt{2\pi m k_b T}} \exp\left(-\frac{\Delta \mathrm{H}^{\ddagger}}{RT}\right) \quad \text{(S13)}$$

Here A_s is the surface area of a single site, which is chosen as 10^{-15} cm^2 (corresponding to a typical site density of 10^{15} cm^{-2}) [29], and m is the molecular mass of the gas species. Note that if $\Delta H^{\ddagger}$ is zero, the sticking coefficient becomes one and the rate coefficient is determined entirely by the frequency of gas molecules hitting free sites on the surface. In the cases where the adsorption rate coefficient is determined by eq. (S13), the desorption rate coefficients are corrected using the equilibrium constant K_{eq}, to ensure thermodynamic consistency.

$$k_{des} = k_{ads}/K_{eq} \quad \text{(S14)}$$

The equilibrium constant, K_{eq}, is calculated as:

$$K_{eq} = \exp\left(-\frac{\Delta G_{ads}}{RT}\right) = \exp\left(-\frac{\Delta H_{ads}}{RT}\right)\exp\left(\frac{\Delta S_{ads}}{R}\right) \quad \text{(S15)}$$

with ΔG_{ads}, ΔH_{ads} and ΔS_{ads} the reaction Gibbs free energy, enthalpy, and entropy, respectively, for adsorption. For all catalyst surface reactions, the Gibbs free reaction energy, ΔG, is calculated as the difference between the Gibbs free energies, G_s, of the products and reactants:

$$\Delta G = \sum_{\substack{s,\\ Products}} G_s - \sum_{\substack{s,\\ Reactants}} G_s \quad \text{(S16)}$$

The Gibbs free activation barrier, $\Delta G^{\ddagger}$, is calculated as the difference between the Gibbs free energies of the transition state (TS) and the reactants, while also considering that the barrier cannot be negative or smaller than the reaction energy:

$$\Delta G^{\ddagger} = \max\left(\left(\sum_{\substack{s,\\ TS}} G_s - \sum_{\substack{s,\\ Reactants}} G_s\right), \Delta G, 0\right) \quad \text{(S17)}$$

in which 'max' denotes the maximum of the three values.

Apart from reactions on the catalyst surface, our model also includes radical loss processes on a non-catalytic surface, like the reactor wall. The rate coefficients for these reactions are calculated as described in section S3.6.

S3.6 Rate coefficients of reactions on the walls

Apart from reactions on the surface of a transition metal catalyst, our model also includes radical recombination on a non-catalytic surface or the reactor walls. This way, radical loss processes on a surface are also included when no catalyst is present in the reactor. Six different types of reactions are included in the surface mechanism [24]. Radicals from the gas-phase can either reversibly adsorb on physisorption sites or irreversibly on chemisorption sites. Physisorbed species can either desorb back to the gas-phase, diffuse to an empty chemisorption site, or diffuse to an occupied chemisorption site and react via a Langmuir-Hinshelwood (L-H) mechanism. Additionally, Eley-Rideal (E-R) reactions, in which a gas species reacts with a chemisorbed species, are also possible [24]. A full list of all wall reactions in the model can be found in Table S9.

The rate coefficients of adsorption for both chemisorption and physisorption are described by the gas kinetics:

$$k = \frac{A_s}{\sqrt{2\pi m k_b T}} \quad \text{(S18)}$$

The site area, A_s, is considered to be the same for both chemisorption and physisorption sites and is chosen equal to 10^{-15} cm^2. This corresponds to a surface site density of 10^{15} cm^{-2} if the surface is entirely covered with sites. Typical surface site densities are in the range of 10^{15}-10^{16} cm^{-2} [24]. The rate coefficient for desorption from physisorption sites is given by [24]:

$$k = \nu_d \exp\left(-\frac{E_d}{RT}\right) \tag{S19}$$

Here ν_d is the frequency factor for vibration of the physisorbed species in the direction perpendicular to the surface, and is set equal to 10^{15} s^{-1} based on ref. [24]. E_d is the activation energy for desorption. In ref. [23], a value of 51 kJ/mol is reported for E_d of O* and N* on silica, and 37 kJ/mol for that of H*. In our model we assume E_d = 50 kJ/mol for all species, except H* for which we use 40 kJ/mol.

Rate constants for E-R reactions between chemisorbed and gas species are calculated using the following equation [24]:

$$k = \frac{A_s}{\sqrt{2\pi m k_b T}} \exp\left(-\frac{E_r}{RT}\right) \tag{S20}$$

with E_r the activation barrier for recombination. Typical values of E_r for recombination of O or N are in the range of 14-24 kJ/mol [24]. While recombination reactions in our model occur between other species, we assume a similar value of 20 kJ/mol for E_r if recombination results in the formation of a stable gas molecule. We also consider some reactions, however, where species recombine on the wall to form a radical. In this case we assume the newly formed radical remains bound to the surface and set E_r to zero. The rate coefficient for diffusion is given by [24,30]:

$$k = \frac{\nu_D}{4} \exp\left(-\frac{E_D}{RT}\right) \tag{S21}$$

In this expression, ν_D is the frequency of vibration of the physisorbed species parallel to the surface, which is set equal to 10^{13} s^{-1} [23,24,30]. E_D is the energy barrier for diffusion to an adjacent site and is estimated as $E_D = E_d/2$, in accordance with [23,24]. Finally, the rate coefficient for L-H reactions is calculated using:

$$k = \frac{\nu_D}{4} \exp\left(-\frac{E_D + E_r}{RT}\right) = \frac{\nu_D}{4} \exp\left(-\frac{E_D}{RT}\right) \exp\left(-\frac{E_r}{RT}\right) \tag{S22}$$

The barrier for recombination, E_r, is taken the same as for the corresponding E-R process [24]. As such, we use E_r = 20 kJ/mol in case recombination results in a stable gas molecule, or zero if a radical is formed, which is assumed to remain bound to the surface.

S4. Evolution of radicals with operating time

Fig. S1 illustrates the evolution of the H, CH_3, O and OH radical densities in the plasma following the start of the reaction process. We call this "operating time", to make clear that this is not the residence time of the gas in the plasma. The latter is determined by the gas flow rate and length of the plasma in the reactor, while the operating time is the time as function of which the gas densities and surface coverages change, as discussed in section S3.1. This corresponds to the time that evolves following the start of an experiment, i.e. after turning on the plasma and gas flow. Our current model does not yet consider the filamentary character of a DBD, i.e., occurrence of microdischarge pulses that cause temporal and spatial nonuniformities. Nevertheless, the time evolution of the radicals can still provide useful insight in the interactions between the plasma species and the catalyst, both at short and long timescales. Note that both the horizontal and vertical axes in Fig. S1 are logarithmically scaled.

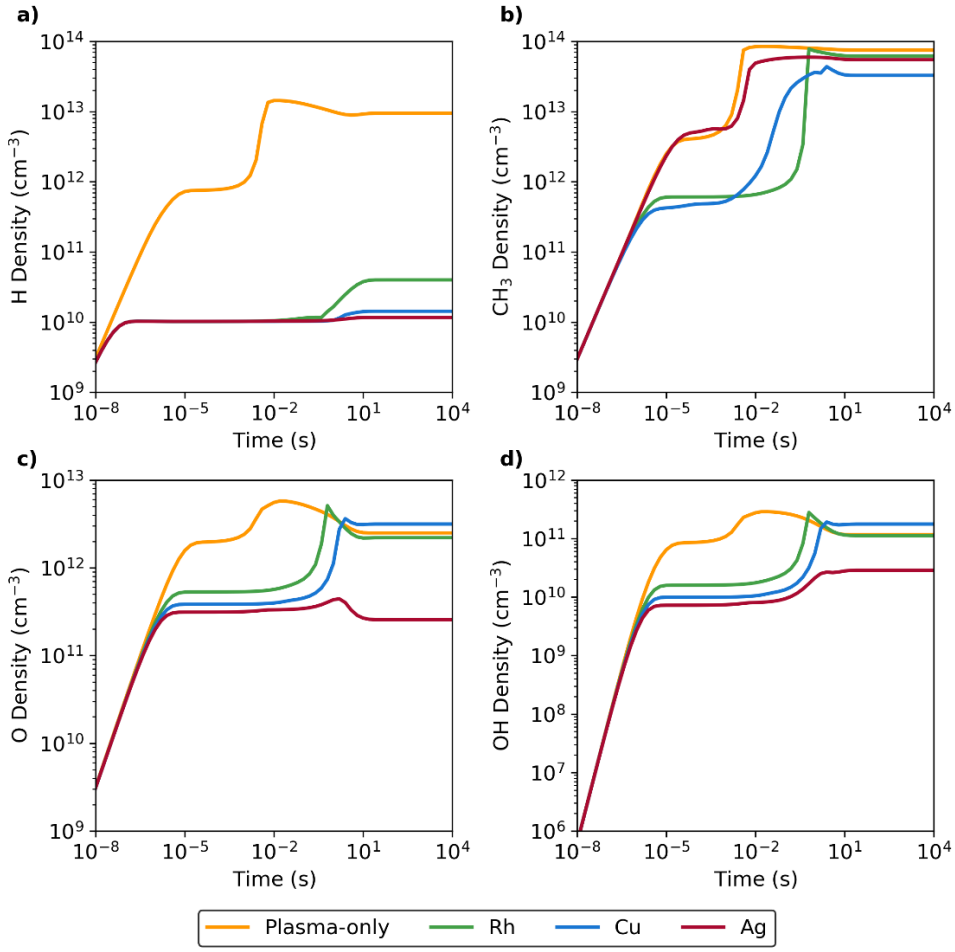

Fig. S1. *Evolution of the (a) H, (b) CH_3, (c) O and (d) OH radical densities with operating time for four different cases, i.e., plasma without catalyst, and plasma combined with a Rh, Cu or Ag catalyst. Calculated for a total pressure of 1 bar and a temperature of 500K.*

Initially, the radical densities clearly increase for all cases, due to electron impact dissociation of the reactant molecules (for the formation of H, CH_3 and O) and subsequent gas-phase reactions (in which also OH is formed). At this timescale, the radical densities are not yet affected by the presence of a transition metal surface and the density curves overlap. At longer timescales, the effect of radical adsorption on the catalyst surface becomes relevant. As a result, the radical densities for the cases without and with different catalysts start to deviate. This occurs between 10^{-8}-10^{-7} s for H radicals (Fig. S1 a)) and around 10^{-6} s for CH_3, O and OH radicals (Fig. S1 b), c) and d), respectively). For the cases with transition metals, most of the radical densities in Fig. S1 show a temporary region of stability. During this period, radical production is partly compensated for by adsorption of radicals on the transition metal surface. As a consequence, the densities of these radicals remain constant as a function of time, and are in general significantly lower when a catalyst is present than in the plasma-only case. However, exceptions also occur, as can be seen in Fig. S1 b) for the CH_3 radicals, when the plasma is combined with Ag. Due to the low adsorption enthalpy of CH_3 on Ag, the density curve for this radical is quite similar to that of the plasma without catalyst. Note that for the plasma-only case, radicals can still recombine on a "non-catalytic" surface, which represents the surface of the reactor wall or a silica packing. However, due to the low densities of chemisorption sites on such a surface and the facile desorption of species from physisorption sites, the rates of radical recombination are typically much lower on the wall compared to on a transition metal surface. Still, exceptions on this do occur when the catalyst is poisoned or for species that bind the transition metal very weakly (like CH_3 on Ag, as explained above).

At timescales of 0.1-1 s, the surfaces of the Cu and Rh catalysts start to become saturated. Due to the drop in the free surface site fractions on these catalysts, less radicals can adsorb on their surfaces and the radical densities in the plasma rise. This is especially visible for CH_3, O and OH in Fig. S1 b), c) and d), respectively, for the cases with Cu and Rh. The rise in CH_3 density starts earlier for the case with Cu, i.e., around 10^{-3}-10^{-2} s. At timescales of 1-10 s, there is again a period of stabilization, and the system typically reaches steady state between 10^{2}-10^{3} s. Depending on the rates of radical recombination on the catalyst surface, the steady-state radical densities can be lower than those in the plasma without catalyst. This is most clear for the H radical densities displayed in Fig. S1 a). The CH_3 densities in Fig. S1 b) show slightly reduced steady-state values for Rh and Ag, compared to plasma without catalyst, while the drop is more significant for Cu. The O and OH densities, on the other hand, are significantly lowered for the case with Ag, as displayed in Fig. S1 c) and d), respectively. For the cases with Rh and Cu, the O and OH densities at steady state are relatively close to those of plasma without catalyst. Note that in the case of Cu, the O and OH densities are slightly higher compared to the plasma-only case, even though these radicals also adsorb on Cu. The reason for this is unclear, but the effect appears to result from a drop in the densities of many other gas species that would otherwise react with O radicals in the

gas-phase. As OH is primarily formed from reaction between O and CH_4 or C_2H_6 in the plasma, the densities of O and OH are coupled.

For the plasma combined with Rh, the radical densities in Fig. S1 b), c) and d) are quite similar to those of the plasma-only case. This is caused by CO* poisoning of the Rh surface at steady state, resulting in partial deactivation of the catalyst. We found this also to be the case for Pt, Pd and Ir, which are not included in Fig. S1. Note that inclusion of lateral interactions between adsorbed CO* might result in partial re-activation of these catalysts. Such interactions are currently not included in our model, as the effect is outside the scope of this study. However, we do expect the global trends to remain valid, i.e., in which the more strongly binding metals are at least partly deactivated due to more difficult desorption. Also note that H radical adsorption and recombination is not affected by the CO* poisoning of the Rh surface, which is a consequence of the separate adsorption site for H* used in our model. In other words, it results from the assumed negligible interactions between the small H atoms and larger adsorbates. For more information, see section S2.

S5. Tables

S5.1 Surface and gas-phase species energies and frequencies

The surface species energies and vibrational frequencies calculated by DFT in our work are listed in Table S1; for the energies and frequencies of other surface species used in the models, we refer to ref. [1]. The adsorbate and transition state energies are given relative to the empty (111) slab and CO, H_2O and H_2 in the gas-phase. In accordance with ref. [1], we use 12 cm^{-1} as a lower limit for the vibrational frequencies and smaller frequencies are replaced with this value. The energies and vibrational frequencies of gas species are listed in Table S2. These energies are not calculated with DFT, but instead we use the experimental enthalpies of formation, which are taken from the NIST chemistry webbook [2]. The zero-point energy (ZPE) and thermodynamic contribution are subtracted from these enthalpies of formation to give the "uncorrected" enthalpies at 0 K. The thermodynamic contribution is estimated from the heat capacity as $c_p(300\ K) \times 300\ K$, with $c_p(300\ K)$ the heat capacity at 300 K [31]. The acquired energies are subsequently recalculated as the formation enthalpies relative to gaseous CO, H_2O and H_2. Note that the energies in Table S2 are only given without the ZPE and thermodynamic contributions, as the "uncorrected" energies are required as input for CatMAP. However, in both CatMAP and our coupled plasma-surface model, the ZPE and thermodynamic contributions are added again to these "uncorrected" energies during the simulations. The vibrational frequencies of the gas species are taken from ref. [32].

Table S1. Energies and vibrational frequencies of surface species on various transition metal (111) surfaces. The energies are calculated as the formation energy of the surface species relative to the empty (111) slab and CO, H_2O and H_2 in the gas-phase.

Species [a]	**Surface**	**Energy (eV)**	**Vibrational frequencies (cm^{-1})** [b]
O^{*s}	Rh	0.42	314.0, 314.0, 461.0
O^{*s}	Ag	1.98	-
O^{*s}	Cu	0.89	-
O^{*s}	Pd	1.01	-
O^{*s}	Pt	1.29	-
O^{*s}	Ir	0.73	-
CO_2^{*s}	Rh	-0.85	12.0, 12.0, 12.0, 37.0, 45.0, 610.0, 620.0, 1311.0, 2343.0
CO_2^{*s}	Ag	-0.82	-
CO_2^{*s}	Cu	-0.83	-
CO_2^{*s}	Pd	-0.84	-
CO_2^{*s}	Pt	-0.85	-
CO_2^{*s}	Ir	-0.85	-
$O\text{-}CO^{*s}$	Rh	0.14	55.0, 117.0, 257.0, 274.0, 383.0, 432.0, 564.0, 1889
$O\text{-}CO^{*s}$	Ag	2.12	-
$O\text{-}CO^{*s}$	Cu	1.02	-
$O\text{-}CO^{*s}$	Pd	0.92	-
$O\text{-}CO^{*s}$	Pt	1.06	-
$O\text{-}CO^{*s}$	Ir	0.13	-
$H\text{-}H^{*h}$	Rh	0.03	85.0, 204.0, 311.0, 1767.0, 1932.0
$H\text{-}H^{*h}$	Ag	1.83	-
$H\text{-}H^{*h}$	Cu	0.98	-
$H\text{-}H^{*h}$	Pd	0.14	-
$H\text{-}H^{*h}$	Pt	0.25	-
$H\text{-}H^{*h}$	Ir	0.11	-
$O\text{-}H^{*s}$	Rh	1.42	111.0, 270.0, 423.0, 459.0, 938.0
$O\text{-}H^{*s}$	Ag	3.22	-
$O\text{-}H^{*s}$	Cu	2.03	-
$O\text{-}H^{*s}$	Pd	1.87	-
$O\text{-}H^{*s}$	Pt	2.11	-
$O\text{-}H^{*s}$	Ir	1.85	-

a) Species containing a hyphen (-) denote transition states.

b) The vibrational frequencies of the species on Rh are used for all descriptor values.

Table S2. Gas-phase species energies and vibrational frequencies.

Species	**Energy (eV)**	**Vibrational frequencies (cm^{-1})**
H_2	0.00	4401.2
H_2O	0.00	3657.0, 1595.0, 3756.0
CH_4	-2.77	2917.0, 1534.0, 1534.0, 3019.0, 3019.0, 3019.0, 1306.0, 1306.0, 1306.0
CO	0.00	2169.8
CO_2	-0.33	1333.0, 2349.0, 667.0, 667.0
CH_2O	-0.28	2782.0, 1746.0, 1500.0, 1167.0, 2843.0, 1249.0
CH_3OH	-1.51	3681.0, 3000.0, 2844.0, 1477.0, 1455.0, 1345.0, 1060.0, 1033.0, 2960.0, 1477.0, 1165.0, 200.0
CH_3CHO	-2.74	3014.0, 2923.0, 2716.0, 1743.0, 1433.0, 1395.0, 1352.0, 1114.0, 867.0, 509.0, 2964.0, 1431.0, 1102.0, 764.0, 150.0
CH_3CH_2OH	-3.71	3652.9, 2984.1, 2939.2, 2899.6, 1490.2, 1463.5, 1411.7, 1371.4, 1256.3, 1090.7, 1027.7, 887.6, 416.5, 2991.4, 2909.6, 1445.8, 1274.8, 1161.0, 811.8, 251.0, 200.0
O	5.32	-
H	2.38	-
CH_3	-0.29	3004.4, 606.5, 3160.8, 3160.8, 1396.0, 1396.0
CH_2	2.39	2805.9, 963.1, 3190.0
OH	3.07	3737.8
CHO	1.56	2434.5, 1868.2, 1080.8

S5.2 Scaling relations

Table S3. Scaling relations that describe the surface species binding energies as function of the binding energies of CH and O* (E_{CH*} and E_{O*}, respectively). All energies are expressed in eV. The binding energies are defined as the formation energies of the adsorbed species relative to the empty (111) slab and CO, H_2O and H_2 in the gas-phase.*

Surface species	**Scaling relation for surface species energy (eV)**
H^{*h}	$0.2157 \times E_{CH*} + 0.0208$
CH_2CO^{*s}	$0.3840 \times E_{CH*} - 2.0507$
CH_2OH^{*s}	$0.4036 \times E_{CH*} - 0.7973$
CH_2O^{*s}	$0.0299 \times E_{CH*} + 0.1287 \times E_{O*} - 0.8431$
CH_2^{*s}	$0.5987 \times E_{CH*} - 0.6190$
$CH_3CH_2OH^{*s}$	$0.0953 \times E_{O*} - 4.247$
CH_3CHOH^{*s}	$0.3899 \times E_{CH*} - 3.0096$
CH_3CHO^{*s}	$0.1068 \times E_{O*} - 3.2775$
CH_3CO^{*s}	$0.4514 \times E_{CH*} - 2.7583$
CH_3O^{*s}	$0.3151 \times E_{O*} - 1.5419$
CH_3^{*s}	$0.2981 \times E_{CH*} - 1.7338$
$CHCO^{*s}$	$0.4047 \times E_{CH*} - 1.6985$
$CHOH^{*s}$	$0.62583 \times E_{CH*} - 0.0469$
CHO^{*s}	$0.4721 \times E_{CH*} - 0.1194$
CH^{*s}	E_{CH*}
CO_2^{*s}	$0.0086 \times E_{CH*} - 0.8335$
CO^{*s}	$0.5075 \times E_{CH*} - 0.8177$
OH^{*s}	$0.3089 \times E_{O*} + 0.2447$
O^{*s}	E_{O*}
$H\text{-}H^{*h}$	$0.4627 \times E_{CH*} + 0.9053$
$CH\text{-}CO^{*s}$	$1.0504 \times E_{CH*} - 0.0304$

CH-H*^{s}	$1.1198 \times E_{CH^*} + 0.5586$
CH-OH*^{s}	$0.8717 \times E_{CH^*} + 0.2692 \times E_{O^*} + 0.9914$
CH_2-H*^{s}	$0.7830 \times E_{CH^*} - 0.1068$
CH_3-CO*^{s}	$0.4927 \times E_{CH^*} - 1.3135$
CH_3-H*^{s}	$0.4721 \times E_{CH^*} - 1.1043$
CH_3-OH*^{s}	$0.1327 \times E_{CH^*} + 0.1939 \times E_{O^*} + 0.0450$
CH_3CHO-H*^{s}	$0.3742 \times E_{CH^*} + 0.0096 \times E_{O^*} - 2.2066$
CH_3CHOH-H *^{s}	$0.4713 \times E_{CH^*} + 0.0211 \times E_{O^*} - 2.5172$
CH_3O-H*^{s}	$0.1085 \times E_{CH^*} + 0.1585 \times E_{O^*} - 0.5971$
H-CH_2CO*^{s}	$0.4969 \times E_{CH^*} - 1.2740$
H-CH_2OH*^{s}	$0.4492 \times E_{CH^*} - 0.1866$
H-CH_2O*^{s}	$0.1947 \times E_{CH^*} + 0.1673 \times E_{O^*} - 0.3649$
H-CH_3CO*^{s}	$0.4777 \times E_{CH^*} + 0.0303 \times E_{O^*} - 2.1454$
H-CHCO*^{s}	$0.6542 \times E_{CH^*} - 0.8822$
H-CHOH*^{s}	$0.6167 \times E_{CH^*} + 0.6003$
H-CHO*^{s}	$0.4828 \times E_{CH^*} + 0.0401 \times E_{O^*} + 0.2964$
H-CO*^{s}	$0.5341 \times E_{CH^*} + 0.1823$
H-OH*^{s}	$0.1497 \times E_{CH^*} + 0.2144 \times E_{O^*} + 0.9553$
HCO-H*^{s}	$0.6838 \times E_{CH^*} + 0.5385$
O-CO*^{s}	$0.2986 \times E_{CH^*} + 0.5883 \times E_{O^*} + 0.5036$
O-H*^{s}	$0.1603 \times E_{CH^*} + 0.7434 \times E_{O^*} + 1.4210$

S5.3 Species included in the model

Table S4. List of the gas-phase species, wall and catalyst surface species included in the model.

Gas-phase species	H_2, H, H_2O, OH, O, CO_2, CO, CH_4, CH_3, CH_2, C_2H_6, C_2H_5, CHO, CH_2O, CH_3O, CH_3OH, CH_2OH, CH_3CH_2OH, CH_3CHO, CH_3CO
Wall species (physisorbed)[a]	$H*^p$, $O*^p$, CH_3*^p, CH_2*^p, $CHO*^p$, $OH*^p$, $*^p$
Wall species (chemisorbed)[a]	$H*^c$, $O*^c$, CH_3*^c, CH_2*^c, $CHO*^c$, $OH*^c$, $*^c$
Catalyst surface species [a]	$H*^h$, $*^h$, $O*^s$, $OH*^s$, CO_2*^s, $CO*^s$, $CHO*^s$, $CHOH*^s$, CH_2OH*^s, CH_2O*^s, CH_3O*^s, $CH*^s$, CH_2*^s, CH_3*^s, $CHCO*^s$, CH_2CO*^s, CH_3CO*^s, CH_3CHO*^s, CH_3CHOH*^s, $CH_3CH_2OH*^s$, $*^s$

a) Superscripts p, c, h and s refer the physisorption, chemisorption, hydrogen reservoir and catalytic surface sites, respectively.

S5.4 Rate coefficients of gas-phase reactions

Table S5 lists the gas-phase reactions and corresponding rate coefficients used in the coupled plasma-surface model, with exception of the electron impact dissociation reactions, which are listed in Table S7 below. Some of the rate coefficients for the dissociation and recombination reactions in Table S5 are given as fall-off expressions of the form [33]:

$$k = \frac{k_0 M k_\infty}{k_0 M + k_\infty} F \tag{S23}$$

$$\log(F) = \frac{\log(F_c)}{1 + \left[\frac{\log(k_0 M / k_\infty)}{N}\right]^2} \tag{S24}$$

$$N = 0.75 - 1.27\log(F_c) \tag{S25}$$

In which k_0 and k_∞ are the low- and high-pressure limit rate coefficients, respectively, F_c is the centered broadening factor and M is the density of neutral gas species, equal to 1.449×10^{19} cm^{-3} at 500 K. Expressions for k_0, k_∞ and F_c are listed in Table S5.

Table S5. List of gas-phase reactions included in the coupled plasma-surface model with the corresponding rate coefficient expressions and references.

Reaction	**Rate coefficient** [a, b]	**Ref.**
$H + OH \rightarrow H_2 + O$	$4.1\times10^{-12}\left(\frac{T}{300}\right)\exp\left(\frac{-3.50\times10^3}{T}\right)$	[34]
$H + OH \rightarrow H_2O$	$6.7\times10^{-31}\left(\frac{T}{300}\right)^{-2.0}\times M$	[34]
$OH + OH \rightarrow H_2O + O$	$1.02\times10^{-12}\left(\frac{T}{300}\right)^{1.4}\exp\left(\frac{2.0\times10^2}{T}\right)$	[28]
$OH \rightarrow O + H$	$4.7\times10^{-8}\left(\frac{T}{300}\right)^{-1.0}\exp\left(\frac{-5.0830\times10^4}{T}\right)\times M$	[34]
$H_2 + OH \rightarrow H + H_2O$	$3.6\times10^{-16}T^{1.52}\exp\left(\frac{-1.74\times10^3}{T}\right)$	[33]
$H_2O + O \rightarrow OH + OH$	$7.6\times10^{-15}T^{1.3}\exp\left(\frac{-8.6\times10^3}{T}\right)$	[28]
$H + H_2O \rightarrow H_2 + OH$	$7.5\times10^{-16}T^{1.6}\exp\left(\frac{-9.03\times10^3}{T}\right)$	[33]
$O + H \rightarrow OH$	$4.33\times10^{-32}\left(\frac{T}{300}\right)^{-1}\times M$	[28]

$H_2 + O \rightarrow H + OH$	$9\times10^{-12}\left(\frac{T}{300}\right)\exp\left(\frac{-4.480\times10^{3}}{T}\right)$	[34]
$H + H \rightarrow H_2$	$1.8\times10^{-30}T^{-1}\times M$	[34]
$CO + O \rightarrow CO_2$	$2.79\times10^{-29}T^{-1.5}\exp\left(\frac{-2.52\times10^{3}}{T}\right)\times M$	[35]
$CH_4 + H \rightarrow CH_3 + H_2$	$6.4\times10^{-18}T^{2.11}\exp\left(\frac{-3.9\times10^{3}}{T}\right)$	[36]
$CH_3 + H_2 \rightarrow CH_4 + H$	$6.62\times10^{-20}T^{2.24}\exp\left(\frac{-3.22\times10^{3}}{T}\right)$	[36]
$CH_3 + H \rightarrow CH_2 + H_2$	$2.1\times10^{-8}T^{-0.56}\exp\left(\frac{-8.0\times10^{3}}{T}\right)$	[33]
$CH_3 + H \rightarrow CH_4$	$k_0 = 1.7\times10^{-24}T^{-1.8}$ $k_\infty = 3.5\times10^{-10}$ $F_c = 6.3\times10^{-1}\exp\left(\frac{-T}{3.3150\times10^{3}}\right)$ $+3.7\times10^{-1}\exp\left(\frac{-T}{6.10\times10^{1}}\right)$	[33] [c]
$CH_2 + H_2 \rightarrow CH_3 + H$	$7.32\times10^{-19}T^{2.3}\exp\left(\frac{-3.6990\times10^{3}}{T}\right)$	[37]
$CH_3 + CH_4 \rightarrow C_2H_6 + H$	$\frac{8\times10^{13}}{N_A}\exp\left(\frac{-1.6736\times10^{5}}{RT}\right)$	[38]
$CH_3 + CH_4 \rightarrow C_2H_5 + H_2$	$\frac{1\times10^{13}}{N_A}\exp\left(\frac{-9.6232\times10^{4}}{RT}\right)$	[38]
$CH_2 + CH_4 \rightarrow CH_3 + CH_3$	$7.14\times10^{-12}\exp\left(\frac{-4.199\times10^{4}}{RT}\right)$	[39]
$CH_3 + CH_3 \rightarrow C_2H_6$	$k_0 = 3.5\times10^{-7}T^{-7}\exp\left(\frac{-1.39\times10^{3}}{T}\right)$ $k_\infty = 6\times10^{-11}$ $F_c = 3.8\times10^{-1}\exp\left(\frac{-T}{7.3\times10^{1}}\right)$ $+6.2\times10^{-1}\exp\left(\frac{-T}{1.18\times10^{3}}\right)$	[33] [c]
$CH_3 + CH_3 \rightarrow C_2H_5 + H$	$9\times10^{-11}\exp\left(\frac{-8.08\times10^{3}}{T}\right)$	[33]
$CH_3 + CH_3 \rightarrow CH_2 + CH_4$	$5.6\times10^{-17}T^{1.34}\exp\left(\frac{-6.791\times10^{4}}{RT}\right)$	[40]

$CH_3 \rightarrow CH_2 + H$	$1.7\times10^{-8}\exp\left(\frac{-4.560\times10^{4}}{T}\right)\times M$	[33]
$C_2H_6 + H \rightarrow C_2H_5 + H_2$	$1.63\times10^{-10}\exp\left(\frac{-4.640\times10^{3}}{T}\right)$	[33]
$C_2H_5 + H_2 \rightarrow C_2H_6 + H$	$5.1\times10^{-24}T^{3.6}\exp\left(\frac{-4.253\times10^{3}}{T}\right)$	[33]
$C_2H_5 + H \rightarrow CH_3 + CH_3$	7×10^{-11}	[33]
$C_2H_5 + H \rightarrow C_2H_6$	$\frac{6\times10^{-11}}{1+10^{-1.915+2.69\times10^{-3}T-2.35\times10^{-7}T^2}}$	[28]
$C_2H_6 + CH_3 \rightarrow C_2H_5 + CH_4$	$9.3\times10^{-14}\exp\left(\frac{-4.740\times10^{3}}{T}\right)$ $+1.4\times10^{-9}\exp\left(\frac{-1.120\times10^{4}}{T}\right)$	[33]
$C_2H_6 + CH_2 \rightarrow C_2H_5 + CH_3$	$\frac{6.5\times10^{12}}{N_A}\exp\left(\frac{-3.31\times10^{4}}{RT}\right)$	[39]
$C_2H_5 + CH_4 \rightarrow C_2H_6 + CH_3$	$1.43\times10^{-25}T^{4.14}\exp\left(\frac{-6.322\times10^{3}}{T}\right)$	[28]
$C_2H_5 + CH_3 \rightarrow C_2H_6 + CH_2$	$3\times10^{-44}T^{9.0956}$	[41]
$CO_2 + H \rightarrow CO + OH$	$4.7\times10^{-10}\exp\left(\frac{-1.3915\times10^{4}}{T}\right)$	[33]
$CO + H \rightarrow CHO$	$2\times10^{-35}T^{0.2}\times M$	[33]
$CO + OH \rightarrow CO_2 + H$	$\frac{3.3\times10^{6}}{N_A}T^{1.55}\exp\left(\frac{4.02\times10^{2}}{T}\right)$	[42]
$CH_4 + O \rightarrow CH_3 + OH$	$7.3\times10^{-19}T^{2.5}\exp\left(\frac{-3.310\times10^{3}}{T}\right)$	[33]
$CH_3 + O \rightarrow H + CH_2O$	$0.8\times1.4\times10^{-10}$	[33]
$CH_3 + O \rightarrow CO + H_2 + H$	$0.2\times1.4\times10^{-10}$	[33]
$CH_2 + O \rightarrow CO + H + H$	$0.6\times3.4\times10^{-10}\exp\left(\frac{-2.7\times10^{2}}{T}\right)$	[33]
$CH_2 + O \rightarrow CO + H_2$	$0.4\times3.4\times10^{-10}\exp\left(\frac{-2.7\times10^{2}}{T}\right)$	[33]
$CH_3 + CO \rightarrow CH_3CO$	$k_0 = 1.6\times10^{-37}T^{1.05}\exp\left(\frac{-1.3\times10^{3}}{T}\right)$ $k_\infty = 3.1\times10^{-16}T^{1.05}\exp\left(\frac{-2.85\times10^{3}}{T}\right)$ $F_c = 5\times10^{-1}$	[33] [c]

$CH_2 + CO_2 \rightarrow CO + CH_2O$	3.9×10^{-14}	[28]
$CH_4 + OH \rightarrow CH_3 + H_2O$	$1.66\times10^{-18}T^{2.182}\exp\left(\frac{-1.231\times10^{3}}{T}\right)$	[43]
$CH_3 + OH \rightarrow CH_3OH$	$k_0 = 1.06\times10^{-10}T^{-6.21}\exp\left(\frac{-6.71\times10^{2}}{T}\right)$ $k_\infty = 7.2\times10^{-9}T^{-0.79}$ $F_c = 7.5\times10^{-1}\exp\left(\frac{-T}{2.1\times10^{2}}\right)$ $+2.5\times10^{-1}\exp\left(\frac{-T}{1.434\times10^{3}}\right)$	[33] [c]
$CH_3 + OH \rightarrow CH_2 + H_2O$	$\frac{k}{M}$ $k_0 = 1.8\times10^{-8}T^{-0.91}\exp\left(\frac{-2.75\times10^{2}}{T}\right)$ $k_\infty = 6.4\times10^{-8}T^{5.8}\exp\left(\frac{4.85\times10^{2}}{T}\right)$ $F_c = 6.64\times10^{-1}\exp\left(\frac{-T}{3.569\times10^{3}}\right)$ $+3.36\times10^{-1}\exp\left(\frac{-T}{1.08\times10^{2}}\right)$ $+\exp\left(\frac{-3.24\times10^{3}}{T}\right)$	[33] [c]
$CH_3 + OH \rightarrow CH_2OH + H$	$1.2\times10^{-12}\exp\left(\frac{-2.76\times10^{3}}{T}\right)$	[33]
$CH_3 + OH \rightarrow CH_3O + H$	$2\times10^{-14}\exp\left(\frac{-6.99\times10^{3}}{T}\right)$	[33]
$CH_3 + OH \rightarrow H_2 + CH_2O$	$5.3\times10^{-15}\exp\left(\frac{-2.53\times10^{3}}{T}\right)$	[33]
$CH_3 + OH \rightarrow CH_4 + O$	$1.16\times10^{-19}T^{2.2}\exp\left(\frac{-2.24\times10^{3}}{T}\right)$	[44]
$CH_3 + H_2O \rightarrow CH_4 + OH$	$8\times10^{-22}T^{2.9}\exp\left(\frac{-7.48\times10^{3}}{T}\right)$	[45]
$CH_2 + OH \rightarrow H + CH_2O$	5×10^{-11}	[28]
$CH_2 + H_2O \rightarrow CH_3 + OH$	1×10^{-16}	[28]
$CH_3O + CO \rightarrow CH_3 + CO_2$	$2.6\times10^{-11}\exp\left(\frac{-5.94\times10^{3}}{T}\right)$	[28]
$H + CHO \rightarrow CO + H_2$	1.5×10^{-10}	[33]

$H + CHO \rightarrow CH_2 + O$	$\frac{3.981\times10^{13}}{N_A}\exp\left(\frac{-4.29\times10^{5}}{RT}\right)$	[46]
$H_2 + CHO \rightarrow H + CH_2O$	$3\times10^{-18}T^{2}\exp\left(\frac{-8.972\times10^{3}}{T}\right)$	[28]
$H + CH_2O \rightarrow H_2 + CHO$	$3.34\times10^{-23}T^{-3.81}\exp\left(\frac{-2.02\times10^{2}}{T}\right)$	[33]
$H + CH_2O \rightarrow CH_3O$	$\frac{2.4\times10^{13}}{N_A}\exp\left(\frac{-1.72\times10^{4}}{T}\right)$	[47]
$CH_3O + H \rightarrow H_2 + CH_2O$	3.3×10^{-11}	[28]
$CH_3O + H \rightarrow CH_3OH$	$3.4\times10^{-10}\left(\frac{T}{300}\right)^{0.33}$	[48]
$CH_3O + H_2 \rightarrow CH_3OH + H$	$1.7\times10^{-15}\left(\frac{T}{300}\right)^{4}\exp\left(\frac{-2.47\times10^{3}}{T}\right)$	[49]
$CH_2OH + H \rightarrow H_2 + CH_2O$	1×10^{-11}	[50]
$CH_2OH + H \rightarrow CH_3 + OH$	1.6×10^{-10}	[50]
$CH_2OH + H_2 \rightarrow CH_3OH + H$	$1.12\times10^{-18}T^{2}\exp\left(\frac{-6.722\times10^{3}}{T}\right)$	[50]
$CH_3OH + H \rightarrow CH_2OH + H_2$	$5.7\times10^{-15}T^{1.24}\exp\left(\frac{-2.26\times10^{3}}{T}\right)$	[33]
$CH_3OH + H \rightarrow CH_3 + H_2O$	1.9×10^{-28}	[51]
$CHO + OH \rightarrow CO + H_2O$	1.8×10^{-10}	[33]
$H_2O + CHO \rightarrow CH_2O + OH$	$3.9\times10^{-16}T^{1.35}\exp\left(\frac{-1.3146\times10^{4}}{T}\right)$	[28]
$CH_2O + OH \rightarrow H_2O + CHO$	$2.31\times10^{-11}\exp\left(\frac{-3.04\times10^{2}}{T}\right)$	[33]
$CH_3O + OH \rightarrow H_2O + CH_2O$	3×10^{-11}	[28]
$CH_2OH + OH \rightarrow H_2O + CH_2O$	4×10^{-11}	[50]
$CH_2OH + H_2O \rightarrow CH_3OH + OH$	$4.2\times10^{-14}\left(\frac{T}{300}\right)^{3.0}\exp\left(\frac{-10440}{T}\right)$	[49]
$CH_3OH + OH \rightarrow H + H_2O + CH_2O$	$2.96\times10^{-16}T^{1.4434}\exp\left(\frac{-5.7\times10^{1}}{T}\right)$	[52]
$CHO + O \rightarrow CO + OH$	5×10^{-11}	[28]
$CHO + O \rightarrow CO_2 + H$	5×10^{-11}	[28]
$CH_2O + O \rightarrow CHO + OH$	$6.9\times10^{-13}T^{0.57}\exp\left(\frac{-1.39\times10^{3}}{T}\right)$	[33]

$CH_3O + O \rightarrow CH_2O + OH$	$0.25\times2.5\times10^{-11}$	[33]
$CH_3OH + O \rightarrow CH_2OH + OH$	$4.1\times10^{-11}\exp\left(\frac{-2.67\times10^{3}}{T}\right)$	[33]
$CH_4 + CHO \rightarrow CH_3 + CH_2O$	$1.21\times10^{-20}T^{2.85}\exp\left(\frac{-1.133\times10^{4}}{T}\right)$	[28]
$CH_3 + CHO \rightarrow CH_4 + CO$	2×10^{-10}	[28]
$CH_3 + CHO \rightarrow CH_3CHO$	3×10^{-11}	[28]
$CH_2 + CHO \rightarrow CH_3 + CO$	3×10^{-11}	[28]
$CH_3 + CH_2O \rightarrow CH_4 + CHO$	$5.3\times10^{-23}T^{3.36}\exp\left(\frac{-2.17\times10^{3}}{T}\right)$	[33]
$CH_2 + CH_2O \rightarrow CH_3 + CHO$	1×10^{-14}	[28]
$CH_3O + CH_4 \rightarrow CH_3 + CH_3OH$	$2.6\times10^{-13}\exp\left(\frac{-4.45\times10^{3}}{T}\right)$	[28]
$CH_3 + CH_3O \rightarrow CH_4 + CH_2O$	4×10^{-11}	[28]
$CH_2 + CH_3O \rightarrow CH_3 + CH_2O$	3×10^{-11}	[28]
$CH_2OH + CH_4 \rightarrow CH_3 + CH_3OH$	$3.6\times10^{-23}T^{3.1}\exp\left(\frac{-8.166\times10^{3}}{T}\right)$	[50]
$CH_2OH + CH_3 \rightarrow CH_3CH_2OH$	2×10^{-11}	[50]
$CH_2OH + CH_3 \rightarrow CH_4 + CH_2O$	4×10^{-12}	[50]
$CH_2 + CH_2OH \rightarrow CH_3 + CH_2O$	2×10^{-12}	[50]
$CH_3 + CH_3OH \rightarrow CH_2OH + CH_4$	$0.33\times5\times10^{-23}T^{3.45}\exp\left(\frac{-4.02\times10^{3}}{T}\right)$	[33]
$CH_3 + CH_3OH \rightarrow CH_3O + CH_4$	$0.67\times5\times10^{-23}T^{3.45}\exp\left(\frac{-4.02\times10^{3}}{T}\right)$	[33]
$CH_2 + CH_3OH \rightarrow CH_2OH + CH_3$	$5.3\times10^{-23}T^{3.2}\exp\left(\frac{-3.609\times10^{3}}{T}\right)$	[50]
$CH_2 + CH_3OH \rightarrow CH_3 + CH_3O$	$2.4\times10^{-23}T^{3.1}\exp\left(\frac{-3.49\times10^{3}}{T}\right)$	[50]
$CHO + CHO \rightarrow CO + CH_2O$	$0.853\times5\times10^{-11}$	[33]
$CHO + CHO \rightarrow CO + CO + H_2$	$0.147\times5\times10^{-11}$	[33]
$CH_3O + CHO \rightarrow CH_3OH + CO$	1.5×10^{-10}	[28]
$CH_2OH + CHO \rightarrow CH_3OH + CO$	2×10^{-10}	[50]
$CH_2OH + CHO \rightarrow CH_2O + CH_2O$	3×10^{-10}	[50]

$CH_3OH + CHO \rightarrow CH_2OH + CH_2O$	$1.6\times10^{-20}T^{2.9}\exp\left(\frac{-6.596\times10^{3}}{T}\right)$	[50]
$CH_3OH + CHO \rightarrow CH_3O + CH_2O$	$1.6\times10^{-22}T^{2.9}\exp\left(\frac{-6.596\times10^{3}}{T}\right)$	[50]
$CH_3O + CH_2O \rightarrow CH_3OH + CHO$	$1.7\times10^{-13}\exp\left(\frac{-1.5\times10^{3}}{T}\right)$	[28]
$CH_2OH + CH_2O \rightarrow CH_3OH + CHO$	$9.1\times10^{-21}T^{2.8}\exp\left(\frac{-2.95\times10^{3}}{T}\right)$	[50]
$CH_3O + CH_3O \rightarrow CH_3OH + CH_2O$	1×10^{-10}	[28]
$CH_2OH + CH_3O \rightarrow CH_3OH + CH_2O$	4×10^{-11}	[50]
$CH_3O + CH_3OH \rightarrow CH_2OH + CH_3OH$	$5\times10^{-13}\exp\left(\frac{-2.05\times10^{3}}{T}\right)$	[50]
$CH_2OH + CH_2OH \rightarrow CH_3OH + CH_2O$	8×10^{-12}	[50]
$CH_2OH + CH_3OH \rightarrow CH_3O + CH_3OH$	$1.3\times10^{-14}\exp\left(\frac{-6.07\times10^{3}}{T}\right)$	[50]
$C_2H_6 + OH \rightarrow C_2H_5 + H_2O$	$1.52\times10^{-17}T^{2}\exp\left(\frac{-5\times10^{2}}{T}\right)$	[33]
$C_2H_5 + OH \rightarrow C_2H_6 + O$	$1.7\times10^{-40}T^{8.8}\exp\left(\frac{-2.5\times10^{2}}{T}\right)$	[44]
$C_2H_5 + H_2O \rightarrow C_2H_6 + OH$	$5.6\times10^{-18}T^{1.44}\exp\left(\frac{-1.015\times10^{4}}{T}\right)$	[28]
$C_2H_6 + O \rightarrow C_2H_5 + OH$	$3\times10^{-19}T^{2.8}\exp\left(\frac{-2.92\times10^{3}}{T}\right)$	[33]
$C_2H_5 + O \rightarrow CH_3CHO + H$	$0.4\times2.2\times10^{-10}$	[33]
$C_2H_5 + O \rightarrow CH_3 + CH_2O$	$0.3\times2.2\times10^{-10}$	[33]
$C_2H_6 + CHO \rightarrow C_2H_5 + CH_2O$	$7.8\times10^{-20}T^{2.72}\exp\left(\frac{-9.176\times10^{3}}{T}\right)$	[28]
$C_2H_6 + CH_3O \rightarrow C_2H_5 + CH_3OH$	$4\times10^{-13}\exp\left(\frac{-3.57\times10^{3}}{T}\right)$	[28]
$C_2H_6 + CH_2OH \rightarrow C_2H_5 + CH_3OH$	$3.3\times10^{-22}T^{2.95}\exp\left(\frac{-7.033\times10^{3}}{T}\right)$	[50]
$C_2H_5 + CHO \rightarrow C_2H_6 + CO$	2×10^{-10}	[28]
$C_2H_5 + CH_2O \rightarrow C_2H_6 + CHO$	$9.2\times10^{-21}T^{2.81}\exp\left(\frac{-2.95\times10^{3}}{T}\right)$	[28]
$C_2H_5 + CH_3O \rightarrow C_2H_6 + CH_2O$	4×10^{-11}	[28]
$C_2H_5 + CH_2OH \rightarrow C_2H_6 + CH_2O$	4×10^{-12}	[50]

$C_2H_5 + CH_3OH \rightarrow C_2H_6 + CH_2OH$	$5.3\times10^{-23}T^{3.2}\exp\left(\frac{-4.61\times10^{3}}{T}\right)$	[50]
$C_2H_5 + CH_3OH \rightarrow C_2H_6 + CH_3O$	$2.4\times10^{-23}T^{3.1}\exp\left(\frac{-4.5\times10^{3}}{T}\right)$	[50]
$CH_3CO + H \rightarrow CH_3 + CHO$	$0.65\times\frac{2\times10^{13}}{N_A}$	[53,54]
$CH_3CO + H \rightarrow CH_3CHO$	$6.02\times10^{-11}T^{0.16}$	[55]
$CH_3CO + H_2 \rightarrow CH_3CHO + H$	$6.8\times10^{-18}T^{1.82}\exp\left(\frac{-8.862\times10^{3}}{T}\right)$	[28]
$CH_3CHO + H \rightarrow CH_3CO + H_2$	$2.18\times10^{-19}T^{2.58}\exp\left(\frac{-6.14\times10^{2}}{T}\right)$	[56]
$CH_3CH_2OH + H \rightarrow C_2H_5 + H_2O$	$\frac{5.9\times10^{11}}{N_A}\exp\left(\frac{-1.44\times10^{4}}{RT}\right)$	[57]
$CH_3CHO + OH \rightarrow CH_3CO + H_2O$	$0.93\times4.8\times10^{-16}T^{1.35}\exp\left(\frac{7.92\times10^{2}}{T}\right)$	[33]
$CH_3CO + O \rightarrow CH_3 + CO_2$	$0.75\times3.5\times10^{-10}$	[33]
$CH_3CHO + O \rightarrow CH_3CO + OH$	$\frac{5\times10^{12}}{N_A}\exp\left(\frac{-7.5\times10^{3}}{RT}\right)$	[53]
$CH_3CO + CH_4 \rightarrow CH_3 + CH_3CHO$	$3.6\times10^{-21}T^{2.88}\exp\left(\frac{-1.08\times10^{4}}{T}\right)$	[28]
$CH_3 + CH_3CHO \rightarrow CH_3CO + CH_4$	$0.993\times5.8\times10^{-32}T^{6.21}\exp\left(\frac{-8.2\times10^{2}}{T}\right)$	[33]
$CH_3 + CH_3CHO \rightarrow CH_3 + CH_4 + CO$	$\frac{6.31\times10^{12}}{N_A}T^{0.5}\exp\left(\frac{-4.48\times10^{4}}{RT}\right)$	[58]
$C_2H_6 + CH_3CO \rightarrow C_2H_5 + CH_3CHO$	$3\times10^{-20}T^{2.75}\exp\left(\frac{-8.82\times10^{3}}{T}\right)$	[28]
$C_2H_5 + CH_3CHO \rightarrow C_2H_6 + CH_3CO$	$\frac{1.26\times10^{12}}{N_A}\exp\left(\frac{-3.56\times10^{4}}{RT}\right)$	[59]
$CH_3CO + CHO \rightarrow CH_3CHO + CO$	1.5×10^{-11}	[28]
$CH_3CO + CH_2O \rightarrow CH_3CHO + CHO$	$3\times10^{-13}\exp\left(\frac{-6.5\times10^{3}}{T}\right)$	[28]
$CH_3CO + CH_3O \rightarrow CH_3CHO + CH_2O$	1×10^{-11}	[28]
$CH_3CO + CH_3OH \rightarrow CH_3CHO + CH_2OH$	$8.06\times10^{-21}T^{2.99}\exp\left(\frac{-6.21\times10^{3}}{T}\right)$	[50]
$CH_3CHO + CH_3O \rightarrow CH_3CO + CH_3OH$	$\frac{1.69\times10^{5}}{N_A}T^{2.04}\exp\left(\frac{-9.84\times10^{3}}{RT}\right)$	[60]

	$+\frac{9.62\times10^{3}}{N_A}T^{2.5}\exp\left(\frac{-6.65\times10^{2}}{RT}\right)$	
CHO → CO + H	$6.6\times10^{-11}\exp\left(\frac{-7.82\times10^{3}}{T}\right)\times M$	[33]
CH_2O → H + CHO	$8.09\times10^{-9}\exp\left(\frac{-3.805\times10^{4}}{T}\right)\times M$	[33]
CH_2O → CO + H_2	$4.7\times10^{-9}\exp\left(\frac{-3.211\times10^{4}}{T}\right)\times M$	[33]
CH_3O → H + CH_2O	$6.8\times10^{13}\exp\left(\frac{-1.317\times10^{4}}{T}\right)$	[33]
CH_2OH → H + CH_2O	$k_0=\frac{6.01\times10^{33}}{N_A}T^{-5.39}\exp\left(\frac{-1.51\times10^{5}}{RT}\right)$ $k_\infty=2.8\times10^{14}T^{-0.73}\exp\left(\frac{-1.37\times10^{5}}{RT}\right)$ $F_c=4\times10^{-2}\exp\left(\frac{-T}{6.76\times10^{1}}\right)$ $+9.6\times10^{-1}\exp\left(\frac{-T}{1.855\times10^{3}}\right)$ $+\exp\left(\frac{-7.543\times10^{3}}{T}\right)$	[61] [c]
CH_3OH → CH_3 + OH	$0.8\times k$ $k_0=1.1\times10^{-7}\exp\left(\frac{-3.308\times10^{4}}{T}\right)$ $k_\infty=2.5\times10^{19}T^{-0.94}\exp\left(\frac{-4.703\times10^{4}}{T}\right)$ $F_c=1.8\times10^{-1}\exp\left(\frac{-T}{2\times10^{2}}\right)$ $+8.2\times10^{-1}\exp\left(\frac{-T}{1.438\times10^{3}}\right)$	[33,62] [c]
CH_3OH → CH_2 + H_2O	$0.15\times k$ $k_0=1.1\times10^{-7}\exp\left(\frac{-3.308\times10^{4}}{T}\right)$ $k_\infty=2.5\times10^{19}T^{-0.94}\exp\left(\frac{-4.703\times10^{4}}{T}\right)$ $F_c=1.8\times10^{-1}\exp\left(\frac{-T}{2\times10^{2}}\right)$ $+8.2\times10^{-1}\exp\left(\frac{-T}{1.438\times10^{3}}\right)$	[33,62] [c]

$CH_3OH \rightarrow CH_2OH + H$	$1.64\times10^{7}T^{2.55}\exp\left(\frac{-3.85\times10^{5}}{RT}\right)$	[63]
$CH_3CO \rightarrow CH_3 + CO$	$k_0 = 1\times10^{-8}\exp\left(\frac{-7.08\times10^{3}}{T}\right)$ $k_\infty = 2\times10^{13}\exp\left(\frac{-8.63\times10^{3}}{T}\right)$ $F_c = 5\times10^{-1}$	[33] [c]
$CH_3CHO \rightarrow CH_3CO + H$	$5\times10^{14}\exp\left(\frac{-3.68\times10^{5}}{RT}\right)$	[64]
$CH_3CHO \rightarrow CH_4 + CO$	$1\times10^{15}\exp\left(\frac{-3.56\times10^{5}}{RT}\right)$	[64]
$CH_3CHO \rightarrow CH_3 + CHO$	$2.1\times10^{16}\exp\left(\frac{-4.1135\times10^{4}}{T}\right)$	[33]
$CH_3CH_2OH \rightarrow CH_2OH + CH_3$	$k_0 = \frac{2.88\times10^{85}}{N_A}T^{-18.9}\exp\left(\frac{-5.532\times10^{4}}{T}\right)$ $k_\infty = 5.94\times10^{23}T^{-1.68}\exp\left(\frac{-4.588\times10^{4}}{T}\right)$ $F_c = 5\times10^{-1}\exp\left(\frac{-T}{2\times10^{2}}\right)$ $+5\times10^{-1}\exp\left(\frac{-T}{8.9\times10^{2}}\right)$ $+\exp\left(\frac{-4.6\times10^{3}}{T}\right)$	[65] [c]
$C_2H_6 + H \rightarrow CH_3 + CH_4$	$K_{eq} \times k_{rev}$	[d]
$C_2H_5 + H_2 \rightarrow CH_3 + CH_4$	$K_{eq} \times k_{rev}$	[d]
$CH_2 + H \rightarrow CH_3$	$K_{eq} \times k_{rev}$	[d]
$H + CH_2O \rightarrow CH_3 + O$	$K_{eq} \times k_{rev}$	[d]
$CO + H_2 \rightarrow CH_2 + O$	$K_{eq} \times k_{rev}$	[d]
$CO + CH_2O \rightarrow CH_2 + CO_2$	$K_{eq} \times k_{rev}$	[d]
$CH_3O + H \rightarrow CH_3 + OH$	$K_{eq} \times k_{rev}$	[d]
$H_2 + CH_2O \rightarrow CH_3 + OH$	$K_{eq} \times k_{rev}$	[d]
$H + CH_2O \rightarrow CH_2 + OH$	$K_{eq} \times k_{rev}$	[d]
$CH_3 + CO_2 \rightarrow CH_3O + CO$	$K_{eq} \times k_{rev}$	[d]
$CO + H_2 \rightarrow H + CHO$	$K_{eq} \times k_{rev}$	[d]
$CH_2 + O \rightarrow H + CHO$	$K_{eq} \times k_{rev}$	[d]
$H_2 + CH_2O \rightarrow CH_3O + H$	$K_{eq} \times k_{rev}$	[d]
$CH_3OH \rightarrow CH_3O + H$	$K_{eq} \times k_{rev}$	[d]

$CH_3OH + H \rightarrow CH_3O + H_2$	$K_{eq} \times k_{rev}$	[d]
$H_2 + CH_2O \rightarrow CH_2OH + H$	$K_{eq} \times k_{rev}$	[d]
$CH_3 + H_2O \rightarrow CH_3OH + H$	$K_{eq} \times k_{rev}$	[d]
$CO + H_2O \rightarrow CHO + OH$	$K_{eq} \times k_{rev}$	[d]
$H_2O + CH_2O \rightarrow CH_3O + OH$	$K_{eq} \times k_{rev}$	[d]
$H_2O + CH_2O \rightarrow CH_2OH + OH$	$K_{eq} \times k_{rev}$	[d]
$CH_3OH + OH \rightarrow CH_2OH + H_2O$	$K_{eq} \times k_{rev}$	[d]
$CO + OH \rightarrow CHO + O$	$K_{eq} \times k_{rev}$	[d]
$CO_2 + H \rightarrow CHO + O$	$K_{eq} \times k_{rev}$	[d]
$CHO + OH \rightarrow CH_2O + O$	$K_{eq} \times k_{rev}$	[d]
$CH_2O + OH \rightarrow CH_3O + O$	$K_{eq} \times k_{rev}$	[d]
$CH_2OH + OH \rightarrow CH_3OH + O$	$K_{eq} \times k_{rev}$	[d]
$CH_4 + CO \rightarrow CH_3 + CHO$	$K_{eq} \times k_{rev}$	[d]
$CH_3 + CO \rightarrow CH_2 + CHO$	$K_{eq} \times k_{rev}$	[d]
$CH_3 + CHO \rightarrow CH_2 + CH_2O$	$K_{eq} \times k_{rev}$	[d]
$CH_4 + CH_2O \rightarrow CH_3 + CH_3O$	$K_{eq} \times k_{rev}$	[d]
$CH_3 + CH_2O \rightarrow CH_2 + CH_3O$	$K_{eq} \times k_{rev}$	[d]
$CH_4 + CH_2O \rightarrow CH_2OH + CH_3$	$K_{eq} \times k_{rev}$	[d]
$CH_3 + CH_2O \rightarrow CH_2 + CH_2OH$	$K_{eq} \times k_{rev}$	[d]
$CH_2OH + CH_3 \rightarrow CH_2 + CH_3OH$	$K_{eq} \times k_{rev}$	[d]
$CH_3 + CH_3O \rightarrow CH_2 + CH_3OH$	$K_{eq} \times k_{rev}$	[d]
$CO + CH_2O \rightarrow CHO + CHO$	$K_{eq} \times k_{rev}$	[d]
$CH_3OH + CO \rightarrow CH_3O + CHO$	$K_{eq} \times k_{rev}$	[d]
$CH_3OH + CO \rightarrow CH_2OH + CHO$	$K_{eq} \times k_{rev}$	[d]
$CH_2O + CH_2O \rightarrow CH_2OH + CHO$	$K_{eq} \times k_{rev}$	[d]
$CH_3OH + CH_2O \rightarrow CH_3O + CH_3O$	$K_{eq} \times k_{rev}$	[d]
$CH_3OH + CH_2O \rightarrow CH_2OH + CH_3O$	$K_{eq} \times k_{rev}$	[d]
$CH_3OH + CH_2O \rightarrow CH_2OH + CH_2OH$	$K_{eq} \times k_{rev}$	[d]
$CH_3CHO + H \rightarrow C_2H_5 + O$	$K_{eq} \times k_{rev}$	[d]
$CH_3 + CH_2O \rightarrow C_2H_5 + O$	$K_{eq} \times k_{rev}$	[d]
$C_2H_6 + CO \rightarrow C_2H_5 + CHO$	$K_{eq} \times k_{rev}$	[d]
$C_2H_6 + CH_2O \rightarrow C_2H_5 + CH_3O$	$K_{eq} \times k_{rev}$	[d]
$C_2H_6 + CH_2O \rightarrow C_2H_5 + CH_2OH$	$K_{eq} \times k_{rev}$	[d]
$CH_3 + CHO \rightarrow CH_3CO + H$	$K_{eq} \times k_{rev}$	[d]
$C_2H_5 + H_2O \rightarrow CH_3CH_2OH + H$	$K_{eq} \times k_{rev}$	[d]

$CH_3CO + H_2O \rightarrow CH_3CHO + OH$	$K_{eq} \times k_{rev}$	[d]
$CH_3 + CO_2 \rightarrow CH_3CO + O$	$K_{eq} \times k_{rev}$	[d]
$CH_3CO + OH \rightarrow CH_3CHO + O$	$K_{eq} \times k_{rev}$	[d]
$CH_3CHO + CO \rightarrow CH_3CO + CHO$	$K_{eq} \times k_{rev}$	[d]
$CH_3CHO + CHO \rightarrow CH_3CO + CH_2O$	$K_{eq} \times k_{rev}$	[d]
$CH_3CHO + CH_2O \rightarrow CH_3CO + CH_3O$	$K_{eq} \times k_{rev}$	[d]
$CH_2OH + CH_3CHO \rightarrow CH_3CO + CH_3OH$	$K_{eq} \times k_{rev}$	[d]
$CH_3CO + CH_3OH \rightarrow CH_3CHO + CH_3O$	$K_{eq} \times k_{rev}$	[d]
$H + CHO \rightarrow CH_2O$	$K_{eq} \times k_{rev}$	[d]
$CO + H_2 \rightarrow CH_2O$	$K_{eq} \times k_{rev}$	[d]
$H + CH_2O \rightarrow CH_2OH$	$K_{eq} \times k_{rev}$	[d]
$CH_2 + H_2O \rightarrow CH_3OH$	$K_{eq} \times k_{rev}$	[d]
$CH_2OH + H \rightarrow CH_3OH$	$K_{eq} \times k_{rev}$	[d]
$CH_4 + CO \rightarrow CH_3CHO$	$K_{eq} \times k_{rev}$	[d]

a) *Units are s^{-1}, $cm^3\ s^{-1}$ or $cm^6\ s^{-1}$ for unimolecular, bimolecular or trimolecular reactions, respectively.*

b) *$N_A = 6.02214076 \times 10^{23}\ mol^{-1}$, $R = 8.314462618\ J\ mol^{-1}\ K^{-1}$, $M = 1.449 \times 10^{19}\ cm^{-3}$.*

c) *Fall-off expressions, see eqs. (S23), (S24) and (S25).*

d) *Rate coefficient calculated from the equilibrium constants and the rate coefficient of the reverse reaction. Equilibrium constants are calculated from the data in ref.* [66].

S5.5 Electron impact processes included in the Bolsig+ calculations

Table S6. List of electron impact processes used in the calculation of the electron impact dissociation rate coefficients and electron mobilities with BOLSIG+.

Electron impact process	**Reference**
$CH_4 + e^- \rightarrow CH_4^+ + 2e^-$	[67]
$CH_4 + e^- \rightarrow CH_3^+ + H + 2e^-$	[67]
$CH_4 + e^- \rightarrow CH_2^+ + H_2 + 2e^-$	[67]
$CH_4 + e^- \rightarrow CH_2^+ + 2H + 2e^-$	[67]
$CH_4 + e^- \rightarrow CH^+ + H_2 + H + 2e^-$	[67]
$CH_4 + e^- \rightarrow CH_3 + H + e^-$	[67]
$CH_4 + e^- \rightarrow CH_2 + H_2 + e^-$	[67]
$CH_4 + e^- \rightarrow CH_2 + 2H + e^-$	[67]
$CH_4 + e^- \rightarrow CH + H_2 + H + e^-$	[67]
$CH_4 + e^- \rightarrow C + H_2 + 2H + e^-$	[67]
$CH_4 + e^- \rightarrow C + 2H_2 + e^-$	[67]
$CH_4 + e^- \rightarrow CH_4 + e^-$ (elastic)	[68]
$CH_4 + e^- \rightarrow CH_4(\nu_{1,3}) + e^-$	[68]
$CH_4 + e^- \rightarrow CH_4(\nu_{2,4}) + e^-$	[68]
$CH_4 + e^- \rightarrow CH_2^- + H_2$	[68]
$CH_4 + e^- \rightarrow CH_3 + H^-$	[68]
$CO_2 + e^- \rightarrow CO_2^+ + 2e^-$	[68]
$CO_2 + e^- \rightarrow CO + O(1D) + e^-$	[69]
$CO_2 + e^- \rightarrow CO(a3P) + O + e^-$	[69]
$CO_2 + e^- \rightarrow CO_2 + e^-$ (effective)	[68]
$CO_2 + e^- \rightarrow CO_2(\nu_{010}) + e^-$	[68]
$CO_2 + e^- \rightarrow CO_2(\nu_{020}) + e^-$	[68]
$CO_2 + e^- \rightarrow CO_2(\nu_{100}) + e^-$	[68]
$CO_2 + e^- \rightarrow CO_2(\nu_{030+110}) + e^-$	[68]
$CO_2 + e^- \rightarrow CO_2(\nu_{001}) + e^-$	[68]
$CO_2 + e^- \rightarrow CO_2(\nu_{040+120+011}) + e^-$	[68]
$CO_2 + e^- \rightarrow CO_2(X, \nu_{020}) + e^-$	[68]
$CO_2 + e^- \rightarrow CO_2(X, \nu_{050+210+130+021+101}) + e^-$	[68]
$CO_2 + e^- \rightarrow CO_2(X, \nu_{300}) + e^-$	[68]
$CO_2 + e^- \rightarrow CO_2(X, \nu_{060+220+140}) + e^-$	[68]

$CO_2 + e^- \rightarrow CO_2(X, \nu_{0n0+n00}) + e^-$	[68]
$CO_2 + e^- \rightarrow CO_2(E1) + e^-$	[68]
$CO_2 + e^- \rightarrow CO_2(E2) + e^-$	[68]
$CO_2 + e^- \rightarrow CO + O^-$	[70]
$CO + e^- \rightarrow CO^+ + 2e^-$	[68]
$CO + e^- \rightarrow C + O + e^-$	[68]
$CO + e^- \rightarrow CO + e^-$ (elastic)	[68]
$CO + e^- \rightarrow CO(\nu_x) + e^-$ (with x = 1-10)	[68]
$CO + e^- \rightarrow CO(a3P) + e^-$	[68]
$CO + e^- \rightarrow CO(a'3Su+) + e^-$	[68]
$CO + e^- \rightarrow CO(A1P) + e^-$	[68]
$CO + e^- \rightarrow CO(b3Su+) + e^-$	[68]
$CO + e^- \rightarrow CO(B1Su+) + e^-$	[68]
$CO + e^- \rightarrow CO(C1Su+) + e^-$	[68]
$CO + e^- \rightarrow CO(E1P) + e^-$	[68]
$CO + e^- \rightarrow C + O^-$	[68]
$C_2H_6 + e^- \rightarrow C_2H_6^+ + 2e^-$	[67]
$C_2H_6 + e^- \rightarrow C_2H_5^+ + H + 2e^-$	[67]
$C_2H_6 + e^- \rightarrow C_2H_4^+ + H_2 + 2e^-$	[67]
$C_2H_6 + e^- \rightarrow C_2H_3^+ + H_2 + H + 2e^-$	[67]
$C_2H_6 + e^- \rightarrow C_2H_2^+ + 2H_2 + 2e^-$	[67]
$C_2H_6 + e^- \rightarrow C_2H_2^+ + H_2 + 2H + 2e^-$	[67]
$C_2H_6 + e^- \rightarrow C_2H_4 + H_2^+ + 2e^-$	[67]
$C_2H_6 + e^- \rightarrow CH_3^+ + CH_3 + 2e^-$	[67]
$C_2H_6 + e^- \rightarrow C_2H_5 + H + e^-$	[67,71]
$C_2H_6 + e^- \rightarrow C_2H_4 + H_2 + e^-$	[67,71]
$C_2H_6 + e^- \rightarrow C_2H_3 + H_2 + H + e^-$	[67,71]
$C_2H_6 + e^- \rightarrow C_2H_2 + 2H_2 + e^-$	[67,71]
$C_2H_6 + e^- \rightarrow CH_4 + CH_2 + e^-$	[67,71]
$C_2H_6 + e^- \rightarrow 2CH_3 + e^-$	[67,71]
$C_2H_6 + e^- \rightarrow C_2H_6 + e^-$ (elastic)	[72]
$C_2H_6 + e^- \rightarrow C_2H_6(\nu_{1,3}) + e^-$	[72]
$C_2H_6 + e^- \rightarrow C_2H_6(\nu_{2,4}) + e^-$	[72]
$C_2H_6 + e^- \rightarrow C_2H_6(E1) + e^-$	[72]
$C_2H_6 + e^- \rightarrow C_2H_6(E2) + e^-$	[72]

$H_2 + e^- \rightarrow H_2^+ + 2e^-$	[68]
$H_2 + e^- \rightarrow H + H^+ + 2e^-$	[73]
$H_2 + e^- \rightarrow 2H + e^-$	[73]
$H_2 + e^- \rightarrow H_2 + e^-$ (elastic)	[68]
$H_2 + e^- \rightarrow H_2(\nu_x) + e^-$ (with x = 1-3)	[68]
$H_2 + e^- \rightarrow H_2(b3Su) + e^-$	[68]
$H_2 + e^- \rightarrow H_2(B1Su) + e^-$	[68]
$H_2 + e^- \rightarrow H_2(c3Pu) + e^-$	[68]
$H_2 + e^- \rightarrow H_2(a3Sg) + e^-$	[68]
$H_2 + e^- \rightarrow H_2(C1Pu) + e^-$	[68]
$H_2 + e^- \rightarrow H_2(E1Sg, F1Sg) + e^-$	[68]
$H_2 + e^- \rightarrow H_2(e3Su) + e^-$	[68]
$H_2 + e^- \rightarrow H_2(B'1Su) + e^-$	[68]
$H_2 + e^- \rightarrow H_2(D1Pu) + e^-$	[68]
$H_2 + e^- \rightarrow H_2(B''1Su) + e^-$	[68]
$H_2 + e^- \rightarrow H_2(D'1Pu) + e^-$	[68]
$H_2 + e^- \rightarrow H + H^-$	[73]
$H_2O + e^- \rightarrow H_2O^+ + 2e^-$	[74,75]
$H_2O + e^- \rightarrow H + OH^+ + 2e^-$	[74,75]
$H_2O + e^- \rightarrow H_2 + O^+ + 2e^-$	[74,75]
$H_2O + e^- \rightarrow H_2^+ + O + 2e^-$	[74,75]
$H_2O + e^- \rightarrow H^+ + OH + 2e^-$	[74,75]
$H_2O + e^- \rightarrow H + OH + e^-$	[76]
$H_2O + e^- \rightarrow H_2O + e^-$ (elastic)	[72]
$H_2O + e^- \rightarrow H_2O(rot) + e^-$	[74]
$H_2O + e^- \rightarrow H_2O(\nu_{010}) + e^-$	[74]
$H_2O + e^- \rightarrow H_2O(\nu_{100+001}) + e^-$	[74]
$H_2O + e^- \rightarrow H + OH^-$	[74,75]
$H_2O + e^- \rightarrow H_2 + O^-$	[74,76]
$H_2O + e^- \rightarrow H^- + OH$	[74,76]

S5.6 Electron impact dissociation rate coefficients

Table S7. Electron impact dissociation reactions included in the coupled plasma-surface model and the corresponding calculated rate coefficients multiplied with the electron density ($n_e = 10^{14}$ cm^{-3}).

Reaction	**$k \times n_e$ (s^{-1})**
$CH_4 + e^- \rightarrow CH_3 + H + e^-$	4.1×10^{-2}
$CH_4 + e^- \rightarrow CH_2 + H_2 + e^-$	9.2×10^{-3}
$CH_4 + e^- \rightarrow CH_2 + 2H + e^-$	6.9×10^{-4}
$CO_2 + e^- \rightarrow CO + O + e^-$	4.4×10^{-2}
$H_2O + e^- \rightarrow H + OH + e^-$	8.2×10^{-2}
$H_2 + e^- \rightarrow 2H + e^-$	9.3×10^{-2}
$C_2H_6 + e^- \rightarrow C_2H_5 + H + e^-$	1.1×10^{-2}
$C_2H_6 + e^- \rightarrow CH_2 + CH_4 + e^-$	4.1×10^{-3}
$C_2H_6 + e^- \rightarrow 2CH_3 + e$	5.9×10^{-3}

S5.7 Catalyst surface reactions

Table S8. List of catalyst surface reactions included in the CatMAP and coupled plasma-surface models.

Reaction[a, b]	**Transition state**
$CH_4 + *^s + *^h \rightleftharpoons CH_3*^s + H*^h$	$CH_3\text{-}H*^s + *^h$
$CH_3*^s + *^h \rightleftharpoons CH_2*^s + H*^h$	$CH_2\text{-}H*^s + *^h$
$CH_2*^s + *^h \rightleftharpoons CH*^s + H*^h$	$CH\text{-}H*^s + *^h$
$CO_2 + *^s \rightleftharpoons CO_2*^s$	-[c]
$CO_2*^s + *^s \rightleftharpoons CO*^s + O*^s$	$O\text{-}CO*^s + *^s$
$CO + *^s \rightleftharpoons CO*^s$	-[c]
$H_2 + *^h + *^h \rightleftharpoons H*^h + H*^h$	$H\text{-}H*^h + *^h$
$O*^s + H*^h \rightleftharpoons OH*^s + *^h$	$O\text{-}H*^s + *^h$
$OH*^s + H*^h \rightleftharpoons H_2O + *^s + *^h$	$H\text{-}OH*^s + *^h$
$H + *^h \rightleftharpoons H*^h$	-[c]
$O + *^s \rightleftharpoons O*^s$	-[c]
$CH_3 + *^s \rightleftharpoons CH_3*^s$	-[c]
$CH_2 + *^s \rightleftharpoons CH_2*^s$	-[c, d]
$OH + *^s \rightleftharpoons OH*^s$	-[c, d]
$CHO + *^s \rightleftharpoons CHO*^s$	-[c, d]
$CO*^s + H*^h \rightleftharpoons CHO*^s + *^h$	$H\text{-}CO*^s + *^h$
$CHO*^s + H*^h \rightleftharpoons CHOH*^s + *^h$	$HCO\text{-}H*^s + *^h$
$CHOH*^s + *^s \rightleftharpoons CH*^s + OH*^s$	$CH\text{-}OH*^s + *^s$
$CH*^s + CO*^s \rightleftharpoons CHCO*^s + *^s$	$CH\text{-}CO*^s + *^s$
$CHCO*^s + H*^h \rightleftharpoons CH_2CO*^s + *^h$	$H\text{-}CHCO*^s + *^h$
$CH_2CO*^s + H*^h \rightleftharpoons CH_3CO*^s + *^h$	$H\text{-}CH_2CO*^s + *^h$
$CH_3CO*^s + H*^h \rightleftharpoons CH_3CHO*^s + *^h$	$H\text{-}CH_3CO*^s + *^h$
$CH_3CHO*^s \rightleftharpoons CH_3CHO + *^s$	-[c]
$CH_3CHO*^s + H*^h \rightleftharpoons CH_3CHOH*^s + *^h$	$CH_3CHO\text{-}H*^s + *^h$
$CH_3CHOH*^s + H*^h \rightleftharpoons CH_3CH_2OH*^s + *^h$	$CH_3CHOH\text{-}H*^s + *^h$
$CH_3CH_2OH*^s \rightleftharpoons CH_3CH_2OH + *^s$	-[c]
$CHO*^s + H*^h \rightleftharpoons CH_2O*^s + *^h$	$H\text{-}CHO*^s + *^h$
$CH_2O*^s \rightleftharpoons CH_2O + *^s$	-[c, d]
$CH_2O*^s + H*^h \rightleftharpoons CH_3O*^s + *^h$	$H\text{-}CH_2O*^s + *^h$
$CH_3O*^s + H*^h \rightleftharpoons CH_3OH + *^s + *^h$	$CH_3O\text{-}H*^s + *^h$

$CHOH^{*s} + H^{*h} \rightleftharpoons CH_2OH^{*s} + *^{h}$	$H\text{-}CHOH^{*s} + *^{h}$
$CH_2OH^{*s} + H^{*h} \rightleftharpoons CH_3OH + *^{s} + *^{h}$	$H\text{-}CH_2OH^{*s} + *^{h}$
$CH_3O^{*s} + *^{s} + H^{*h} \rightleftharpoons CH_3^{*s} + OH^{*s} + *^{h}$	$CH_3\text{-}OH^{*s} + *^{s} + *^{h}$
$CH_3^{*s} + CO^{*s} \rightleftharpoons CH_3CO^{*s} + *^{s}$	$CH_3\text{-}CO^{*s} + *^{s}$

a) All reactions on the transition metal surfaces are included in both the forward and reverse direction.

b) Superscripts h and s denote hydrogen reservoir and catalytic surface sites, respectively.

c) Molecular and radical adsorption/desorption reactions are considered to occur without additional energy barrier. For these cases the enthalpy and Gibbs free energy barriers are determined by the reaction enthalpy and Gibbs free energy, respectively.

d) These adsorption/desorption reactions are only included in the coupled plasma-surface simulations and not in the simulations with the CatMAP model.

S5.8 Reactions on the non-catalytic wall

Table S9. List of reactions that occur on the non-catalytic wall included in the coupled plasma-surface model.

Physisorption [a]	**Desorption** [a]
$H + *^p \rightarrow H*^p$	$H*^p \rightarrow H + *^p$
$O + *^p \rightarrow O*^p$	$O*^p \rightarrow O + *^p$
$CH_3 + *^p \rightarrow CH_3*^p$	$CH_3*^p \rightarrow CH_3 + *^p$
$CH_2 + *^p \rightarrow CH_2*^p$	$CH_2*^p \rightarrow CH_2 + *^p$
$CHO + *^p \rightarrow CHO*^p$	$CHO*^p \rightarrow CHO + *^p$
$OH + *^p \rightarrow OH*^p$	$OH*^p \rightarrow OH + *^p$
Chemisorption [a]	**Surface diffusion** [a]
$H + *^c \rightarrow H*^c$	$H*^p + *^c \rightarrow H*^c + *^p$
$O + *^c \rightarrow O*^c$	$O*^p + *^c \rightarrow O*^c + *^p$
$CH_3 + *^c \rightarrow CH_3*^c$	$CH_3*^p + *^c \rightarrow CH_3*^c + *^p$
$CH_2 + *^c \rightarrow CH_2*^c$	$CH_2*^p + *^c \rightarrow CH_2*^c + *^p$
$CHO + *^c \rightarrow CHO*^c$	$CHO*^p + *^c \rightarrow CHO*^c + *^p$
$OH + *^c \rightarrow OH*^c$	$OH*^p + *^c \rightarrow OH*^c + *^p$
Eley-Rideal [a]	**Langmuir-Hinshelwood** [a]
$H + H*^c \rightarrow H_2 + *^c$	$H*^p + H*^c \rightarrow H_2 + *^p + *^c$
$H + CH_3*^c \rightarrow CH_4 + *^c$	$H*^p + CH_3*^c \rightarrow CH_4 + *^p + *^c$
$H + CHO*^c \rightarrow CH_2O + *^c$	$H*^p + CHO*^c \rightarrow CH_2O + *^p + *^c$
$H + OH*^c \rightarrow H_2O + *^c$	$H*^p + OH*^c \rightarrow H_2O + *^p + *^c$
$H + O*^c \rightarrow OH*^c$	$H*^p + O*^c \rightarrow OH*^c + *^p$
$H + CH_2*^c \rightarrow CH_3*^c$	$H*^p + CH_2*^c \rightarrow CH_3*^c + *^p$
$CH_3 + H*^c \rightarrow CH_4 + *^c$	$CH_3*^p + H*^c \rightarrow CH_4 + *^p + *^c$
$CHO + H*^c \rightarrow CH_2O + *^c$	$CHO*^p + H*^c \rightarrow CH_2O + *^p + *^c$
$OH + H*^c \rightarrow H_2O + *^c$	$OH*^p + H*^c \rightarrow H_2O + *^p + *^c$
$O + H*^c \rightarrow OH*^c$	$O*^p + H*^c \rightarrow OH*^c + *^p$
$CH_2 + H*^c \rightarrow CH_3*^c$	$CH_2*^p + H*^c \rightarrow CH_3*^c + *^p$
$CO + O*^c \rightarrow CO_2 + *^c$	

a) Superscripts c and p denote chemisorption and physisorption sites, respectively.

S6. References

[1] J. Schumann, A.J. Medford, J.S. Yoo, Z.-J. Zhao, P. Bothra, A. Cao, F. Studt, F. Abild-Pedersen, J.K. Nørskov, ACS Catal. 8 (2018) 3447–3453. https://doi.org/10.1021/acscatal.8b00201.

[2] P.J. Linstrom, W.G. Mallard, eds., NIST Chemistry WebBook, NIST Standard Reference Database Number 69, National Institute of Standards and Technology, Gaithersburg MD, 20899, . https://doi.org/10.18434/T4D303.

[3] J. Klimeš, D.R. Bowler, A. Michaelides, Phys. Rev. B. 83 (2011) 195131. https://doi.org/10.1103/PhysRevB.83.195131.

[4] G. Kresse, J. Hafner, Phys. Rev. B. 49 (1994) 14251–14269. https://doi.org/10.1103/PhysRevB.49.14251.

[5] G. Kresse, J. Hafner, Phys. Rev. B. 47 (1993) 558–561. https://doi.org/10.1103/PhysRevB.47.558.

[6] G. Kresse, J. Furthmüller, Comput. Mater. Sci. 6 (1996) 15–50. https://doi.org/10.1016/0927-0256(96)00008-0.

[7] G. Kresse, J. Furthmüller, Phys. Rev. B. 54 (1996) 11169–11186. https://doi.org/10.1103/PhysRevB.54.11169.

[8] G. Román-Pérez, J.M. Soler, Phys. Rev. Lett. 103 (2009) 096102. https://doi.org/10.1103/PhysRevLett.103.096102.

[9] K. Lee, É.D. Murray, L. Kong, B.I. Lundqvist, D.C. Langreth, Phys. Rev. B. 82 (2010) 081101. https://doi.org/10.1103/PhysRevB.82.081101.

[10] J. Wellendorff, K.T. Lundgaard, A. Møgelhøj, V. Petzold, D.D. Landis, J.K. Nørskov, T. Bligaard, K.W. Jacobsen, Phys. Rev. B. 85 (2012) 235149. https://doi.org/10.1103/PhysRevB.85.235149.

[11] G. Kresse, J. Hafner, J. Phys. Condens. Matter. 6 (1994) 8245–8257. https://doi.org/10.1088/0953-8984/6/40/015.

[12] G. Kresse, D. Joubert, Phys. Rev. B. 59 (1999) 1758–1775. https://doi.org/10.1103/PhysRevB.59.1758.

[13] G. Henkelman, H. Jónsson, J. Chem. Phys. 111 (1999) 7010–7022. https://doi.org/10.1063/1.480097.

[14] A. Heyden, A.T. Bell, F.J. Keil, J. Chem. Phys. 123 (2005) 224101. https://doi.org/10.1063/1.2104507.

[15] J. Kästner, P. Sherwood, J. Chem. Phys. 128 (2008) 014106. https://doi.org/10.1063/1.2815812.

[16] P. Xiao, D. Sheppard, J. Rogal, G. Henkelman, J. Chem. Phys. 140 (2014) 174104. https://doi.org/10.1063/1.4873437.

[17] A.J. Medford, C. Shi, M.J. Hoffmann, A.C. Lausche, S.R. Fitzgibbon, T. Bligaard, J.K. Nørskov, Catal. Letters. 145 (2015) 794–807. https://doi.org/10.1007/s10562-015-1495-6.

[18] F. Abild-Pedersen, J. Greeley, F. Studt, J. Rossmeisl, T.R. Munter, P.G. Moses, E. Skúlason, T. Bligaard, J.K. Nørskov, Phys. Rev. Lett. 99 (2007) 016105. https://doi.org/10.1103/PhysRevLett.99.016105.

[19] S. Wang, B. Temel, J. Shen, G. Jones, L.C. Grabow, F. Studt, T. Bligaard, F. Abild-Pedersen, C.H. Christensen, J.K. Nørskov, Catal. Letters. 141 (2011) 370–373. https://doi.org/10.1007/s10562-010-0477-y.

[20] A.C. Lausche, A.J. Medford, T.S. Khan, Y. Xu, T. Bligaard, F. Abild-Pedersen, J.K. Nørskov, F. Studt, J. Catal. 307 (2013) 275–282. https://doi.org/10.1016/j.jcat.2013.08.002.

[21] A.H. Larsen, J.J. Mortensen, J. Blomqvist, I.E. Castelli, R. Christensen, M. Dułak, J. Friis, M.N. Groves, B. Hammer, C. Hargus, E.D. Hermes, P.C. Jennings, P.B. Jensen, J. Kermode, J.R. Kitchin, E.L. Kolsbjerg, J. Kubal, K. Kaasbjerg, S. Lysgaard, J. Bergmann Maronsson, T. Maxson, T. Olsen, L. Pastewka, A. Peterson, C. Rostgaard, J. Schiøtz, O. Schütt, M. Strange, K.S. Thygesen, T. Vegge, L. Vilhelmsen, M. Walter, Z. Zeng, K.W. Jacobsen, J. Phys. Condens. Matter. 29 (2017) 273002. https://doi.org/10.1088/1361-648X/aa680e.

[22] P. Mehta, P. Barboun, F.A. Herrera, J. Kim, P. Rumbach, D.B. Go, J.C. Hicks, W.F. Schneider, Nat. Catal. 1 (2018) 269–275. https://doi.org/10.1038/s41929-018-0045-1.

[23] Y.C. Kim, M. Boudart, Langmuir. 7 (1991) 2999–3005. https://doi.org/10.1021/la00060a016.

[24] V. Guerra, IEEE Trans. Plasma Sci. 35 (2007) 1397–1412. https://doi.org/10.1109/TPS.2007.902028.

[25] A.E.D. Heylen, Int. J. Electron. 39 (1975) 653–660. https://doi.org/10.1080/00207217508920532.

[26] A. Fridman, Plasma Chemistry, Cambridge University Press, New York, 2008. www.cambridge.org/9780521847353.

[27] G.J.M. Hagelaar, L.C. Pitchford, Plasma Sources Sci. Technol. 14 (2005) 722–733. https://doi.org/10.1088/0963-0252/14/4/011.

[28] W. Tsang, R.F. Hampson, J. Phys. Chem. Ref. Data. 15 (1986) 1087–1279.

https://doi.org/10.1063/1.555759.

[29] C.T. Campbell, L.H. Sprowl, L. Árnadóttir, J. Phys. Chem. C. 120 (2016) 10283–10297. https://doi.org/10.1021/acs.jpcc.6b00975.

[30] N.E. Afonina, V.G. Gromov, V.L. Kovalev, Fluid Dyn. 37 (2002) 117–125.

[31] A.J. Medford, A.C. Lausche, F. Abild-Pedersen, B. Temel, N.C. Schjødt, J.K. Nørskov, F. Studt, Top. Catal. 57 (2014) 135–142. https://doi.org/10.1007/s11244-013-0169-0.

[32] R.D. Johnson, ed., NIST Computational Chemistry Comparison and Benchmark Database NIST Standard Reference Database Number 101 Release 22, 2022. https://doi.org/10.18434/T47C7Z.

[33] D.L. Baulch, C.T. Bowman, C.J. Cobos, R.A. Cox, T. Just, J.A. Kerr, M.J. Pilling, D. Stocker, J. Troe, W. Tsang, R.W. Walker, J. Warnatz, J. Phys. Chem. Ref. Data. 34 (2005) 757–1397. https://doi.org/10.1063/1.1748524.

[34] M. Capitelli, C.M. Ferreira, B.F. Gordiets, A.I. Osipov, Plasma Kinetics in Atmospheric Gases, Springer Berlin Heidelberg, Berlin, Heidelberg, 2000. https://doi.org/10.1007/978-3-662-04158-1.

[35] H.G. Wagner, F. Zabel, Berichte Der Bunsengesellschaft Für Phys. Chemie. 78 (1974) 705–712. https://doi.org/10.1002/bbpc.19740780717.

[36] M.J. Rabinowitz, J.W. Sutherland, P.M. Patterson, R.B. Klemm, J. Phys. Chem. 95 (1991) 674–681. https://doi.org/10.1021/j100155a033.

[37] K.-W. Lu, H. Matsui, C.-L. Huang, P. Raghunath, N.-S. Wang, M.C. Lin, J. Phys. Chem. A. 114 (2010) 5493–5502. https://doi.org/10.1021/jp100535r.

[38] K. Tabayashi, S.H. Bauer, Combust. Flame. 34 (1979) 63–83. https://doi.org/10.1016/0010-2180(79)90079-8.

[39] T. Böhland, S. Dõbẽ, F. Temps, H.G. Wagner, Berichte Der Bunsengesellschaft Für Phys. Chemie. 89 (1985) 1110–1116. https://doi.org/10.1002/bbpc.19850891018.

[40] P. Han, K. Su, Y. Liu, Y. Wang, X. Wang, Q. Zeng, L. Cheng, L. Zhang, J. Comput. Chem. 32 (2011) 2745–2755. https://doi.org/10.1002/jcc.21854.

[41] Y. Ge, M.S. Gordon, F. Battaglia, R.O. Fox, J. Phys. Chem. A. 114 (2010) 2384–2392. https://doi.org/10.1021/jp911673h.

[42] V. Lissianski, H. Yang, Z. Qin, M.R. Mueller, K.S. Shin, W.C. Gardiner, Chem. Phys. Lett. 240 (1995) 57–62. https://doi.org/10.1016/0009-2614(95)00496-Q.

[43] N.K. Srinivasan, M.-C. Su, J.W. Sutherland, J. V. Michael, J. Phys. Chem. A. 109 (2005) 1857–1863. https://doi.org/10.1021/jp040679j.

[44] N. Cohen, K.R. Westberg, J. Phys. Chem. Ref. Data. 20 (1991) 1211–1311. https://doi.org/10.1063/1.555901.

[45] N. Cohen, K.R. Westberg, J. Phys. Chem. Ref. Data. 12 (1983) 531–590. https://doi.org/10.1063/1.555692.

[46] T. Tsuboi, K. Hashimoto, Combust. Flame. 42 (1981) 61–76. https://doi.org/10.1016/0010-2180(81)90142-5.

[47] H.J. Curran, Int. J. Chem. Kinet. 38 (2006) 250–275. https://doi.org/10.1002/kin.20153.

[48] K. Brudnik, A.A. Gola, J.T. Jodkowski, J. Mol. Model. 15 (2009) 1061–1066. https://doi.org/10.1007/s00894-009-0461-x.

[49] J.T. Jodkowski, M.-T. Rayez, J.-C. Rayez, T. Bérces, S. Dóbé, J. Phys. Chem. A. 103 (1999) 3750–3765. https://doi.org/10.1021/jp984367q.

[50] W. Tsang, J. Phys. Chem. Ref. Data. 16 (1987) 471–508. https://doi.org/10.1063/1.555802.

[51] G. Lendvay, T. Bérces, F. Márta, J. Phys. Chem. A. 101 (1997) 1588–1594. https://doi.org/10.1021/jp963188a.

[52] N.K. Srinivasan, M.-C. Su, J. V. Michael, J. Phys. Chem. A. 111 (2007) 3951–3958. https://doi.org/10.1021/jp0673516.

[53] J. Warnatz, Rate Coefficients in the C/H/O System, in: Combust. Chem., Springer New York, New York, NY, 1984: pp. 197–360. https://doi.org/10.1007/978-1-4684-0186-8_5.

[54] K. Ohmori, A. Miyoshi, H. Matsui, N. Washida, J. Phys. Chem. 94 (1990) 3253–3255. https://doi.org/10.1021/j100371a006.

[55] V.D. Knyazev, Chem. Phys. Lett. 685 (2017) 165–170. https://doi.org/10.1016/j.cplett.2017.07.040.

[56] R. Sivaramakrishnan, J. V. Michael, S.J. Klippenstein, J. Phys. Chem. A. 114 (2010) 755–764. https://doi.org/10.1021/jp906918z.

[57] W.K. Aders, H.G. Wagner, Berichte Der Bunsen-Gesellschaft. 77 (1973) 332–335. https://doi.org/10.1002/bbpc.19730770509.

[58] R.E. Dodd, Trans. Faraday Soc. 47 (1951) 56–62. https://doi.org/10.1039/tf9514700056.

[59] G. Höhlein, G.R. Freeman, J. Am. Chem. Soc. 92 (1970) 6118–6125.

https://doi.org/10.1021/ja00724a004.

[60] X. Zhang, L. Ye, Y. Li, Y. Zhang, C. Cao, J. Yang, Z. Zhou, Z. Huang, F. Qi, Combust. Flame. 191 (2018) 431–441. https://doi.org/10.1016/j.combustflame.2018.01.027.

[61] T.J. Held, F.L. Dryer, Int. J. Chem. Kinet. 30 (1998) 805–830. https://doi.org/10.1002/(SICI)1097-4601(1998)30:11<805::AID-KIN4>3.0.CO;2-Z.

[62] C. Dombrowsky, A. Hoffmann, M. Klatt, H. Gg. Wagner, Berichte Der Bunsengesellschaft Für Phys. Chemie. 95 (1991) 1685–1687. https://doi.org/10.1002/bbpc.19910951217.

[63] W.-C. Ing, C.Y. Sheng, J.W. Bozzelli, Fuel Process. Technol. 83 (2003) 111–145. https://doi.org/10.1016/S0378-3820(03)00062-6.

[64] K. Yasunaga, S. Kubo, H. Hoshikawa, T. Kamesawa, Y. Hidaka, Int. J. Chem. Kinet. 40 (2007) 73–102. https://doi.org/10.1002/kin.20294.

[65] N.M. Marinov, Int. J. Chem. Kinet. 31 (1999) 183–220. https://doi.org/10.1002/(SICI)1097-4601(1999)31:3<183::AID-KIN3>3.0.CO;2-X.

[66] B.J. McBride, M.J. Zehe, S. Gordon, NASA Glenn coefficients for calculating thermodynamic properties of individual species, 2002. https://ntrs.nasa.gov/search.jsp?R=20020085330 2020-05-03T03:42:36+00:00Z.

[67] D. Reiter, R.K. Janev, Contrib. to Plasma Phys. 50 (2010) 986–1013. https://doi.org/10.1002/ctpp.201000090.

[68] IST-Lisbon database. www.lxcat.net (accessed January 4, 2023).

[69] L.S. Polak, D.I. Slovetsky, Int. J. Radiat. Phys. Chem. 8 (1976) 257–282. https://doi.org/10.1016/0020-7055(76)90070-X.

[70] Biagi database. www.lxcat.net (accessed January 4, 2023).

[71] R.K. Janev, D. Reiter, Phys. Plasmas. 11 (2004) 780–829. https://doi.org/10.1063/1.1630794.

[72] Hayashi database. www.lxcat.net (accessed January 3, 2023).

[73] Itikawa database. www.lxcat.net (accessed January 4, 2023).

[74] C. Verheyen, T. Silva, V. Guerra, A. Bogaerts, Plasma Sources Sci. Technol. 29 (2020) 095009. https://doi.org/10.1088/1361-6595/aba1c8.

[75] Y. Itikawa, N. Mason, J. Phys. Chem. Ref. Data. 34 (2005) 1–22. https://doi.org/10.1063/1.1799251.

[76] TRINITI database. www.lxcat.net (accessed January 4, 2023).